Results in Surfaces and Interfaces 16 (2024) 100255

Contents lists available at ScienceDirect

Results in Surfaces and Interfaces

journal homepage: www.elsevier.com/locate/rsurfi

# Development of novel composite materials based on kaolinitic clay modified with ZnO for the elimination of azo dyes by adsorption in water

Pierre Ngue Song [a], Julien G. Mahy [a,*], Antoine Farcy [a], Cédric Calberg [a], Nathalie Fagel [b], Stéphanie D. Lambert [a]

[a] Department of Chemical Engineering – Nanomaterials, Catalysis & Electrochemistry, University of Liège, B6a, Quartier Agora, Allée du Six Août 11, 4000, Liège, Belgium

[b] Laboratoire Argiles, Géochimie et Environnements Sédimentaires (AGEs), Department of Geology, Faculty of Sciences, University of Liège, Liège, B-4000, Belgium

ARTICLE INFO

*Keywords:*
Water treatment
Surface modification
Adsorbent
Natural material valorization
Porous materials

ABSTRACT

In this work, ZnO nanoparticles, synthesized by the sol-gel process, are immobilized on the external surface of raw kaolinite particles and kaolinite activated by different treatments: heat treatment at 600, 700 and 800 °C; treatment in a dimethyl sulfoxide (DMSO) medium; hot acid treatment (HCl, 6M) under reflux conditions or heat treatment at 800 °C followed by acid treatment. Characterization confirmed the successful immobilization of the nanocrystalline ZnO particles in the hexagonal structure of the different clay matrices. Measurement of the zeta potential showed a sudden inversion of the nature of the surface charge of certain composite materials obtained, through zeta potential values ranging from −31 mV before doping with ZnO to +36 mV after doping. The raw kaolinite and certain composites obtained were tested in batch mode for the adsorption in aqueous solution of three anionic azo textile dyes: a monozoic (Mordant Red 19, MR19), diazoic (Direct Blue 53, DB53) and a triazoic (Direct Green 1, DG1) dye. Compared to raw kaolinite, a linear and rapid increase in the quantity of dye adsorbed is observed during the first 5 min with retention rates around 95% for the best composite materials. The adsorption efficiency strongly depends on the zeta potential of the material: the higher the latter is towards positive values, the better the adsorption capacities of the samples towards these anionic textile dyes.

## 1. Introduction

The different techniques and machines available make it possible to dye virtually all types of textile materials at any stage of their manufacturing (fiber, thread, fabric or clothing). The explosion of demographics with an increasing demand for high-end products has forced the textile industry to increase production; this has also boosted the economic sector in the production of cheap synthetic dyes. Thus, annually, more than 700,000 tons of synthetic dyes are produced globally (Artifon et al., 2021; Gou et al., 2022). The category of azo dyes is among the most toxic (Florêncio et al., 2021; Ikram et al., 2022), and more widespread in terms of application in the textile industries. It alone represents more than 50% of global production (Bera and Tank, 2021; Ravadelli et al., 2021).

It is estimated that more than 10–15% of these chemical compounds are discharged into the effluents of textile industries without prior treatment (Dihom et al., 2022; Vaiano et al., 2020). In their structure, azo dyes are designed to be recalcitrant to environmental conditions such as light, temperature, microbial attack and oxidizing agents (Chung, 2016). Furthermore, their presence in aquatic systems, even at low concentrations, is very visible; they reduce light penetration and have a detrimental effect on photosynthesis (Selvaraj et al., 2021; Hernández-Zamora and Martínez-Jerónimo, 2019).

This discharge also represents a potential danger of bioaccumulation that could affect humans through transfer through the food chain (Ahmad et al., 2023; Goud et al., 2020). Numerous studies carried out on azo dyes have demonstrated that these chemical compounds present carcinogenic, mutagenic and teratogenic effects for humans and animals directly or indirectly through their metabolites which are carcinogenic amines (Dihom et al., 2022; Ngo and Tischler, 2022). For this reason, in 2000, the Danish Environmental Protection Agency (DEPA) imposed a concentration limit of 3.1 µg/L of azo dye in drinking water to limit cancer risks (Berkani et al., 2020). The European Commission (according to standard IP/03/11 of January 7, 2003, having taken effect from June 30, 2004) adopted a new directive prohibiting the marketing and use in the European Union of a dangerous azo chemical dye obtained by

* Corresponding author. Allée du Six Août 11, 4000, Liège, Belgium.
*E-mail address:* julien.mahy@uliege.be (J.G. Mahy).

https://doi.org/10.1016/j.rsurfi.2024.100255
Received 29 April 2024; Received in revised form 5 July 2024; Accepted 8 July 2024
Available online 11 July 2024

chromating and used for textiles. According to Annex XVII of the REACH regulation, No. 1907/2006, this prohibited the use of azo dyes deemed dangerous (Brüschweiler and Merlot, 2017).

Water resources decrease as temperatures rise. In a context where water scarcity and droughts are increasingly felt, one of the most sustainable solutions would be to close the water cycle within a factory (Paździor et al., 2019; Ribeiro et al., 2017). Consequently, the depollution of wastewater from textile industries contaminated by azo dyes is necessary for animal and human health and environmental protection, but above all for the possible reuse of this unconventional water. This depollution is a major challenge to be addressed by researchers. Several biological, physical and chemical methods have been implemented for the elimination of azo dyes in aqueous solution with the aim of possible treatment of textile industrial effluents. We can cite, among others, microbial biodegradation (Tizazu et al., 2023), advanced oxidation processes (AOP) (Paquini et al., 2023), coagulation flocculation (Han et al., 2022), membrane filtration (Benkhaya et al., 2021) and adsorption (Brinza et al., 2022; Khader et al., 2023). However, most of these technologies are expensive from the point of view of their implementation and especially when they are applied to high flow industrial effluents. Only the adsorption technique seems to be well suited to the textile industry (Carmen and Daniela, 2012), given its proven effectiveness in the elimination of organic pollutants and also for economic considerations.

Numerous works on the adsorption, or even comparative studies of adsorption, of anionic azo dyes in aqueous solution using natural kaolinitic clay as an adsorbent matrix have been carried out over the last decade (Aragaw and Alene, 2022; Fumba et al., 2014; Paredes-Quevedo et al., 2021). However, the results obtained are insufficient because the quantities adsorbed at equilibrium are low (<5 mg/g). These low values of adsorption at equilibrium could be explained by the fact that kaolinites are non-swelling clays (He et al., 2013), having a low cation exchange capacity (CEC) (3–15 meq/(100 g)) (Vane and Zang, 1997), low porosity (Turer, 2007) and finally a small specific surface area varying from 10 to 30 $m^2/g$ (Kahr and Madsen, 1995; Song et al., 2023). On the other hand, the surface charge of kaolinite is an important factor that can also explain the poor interaction between the clay and the anionic molecules of azo dyes in aqueous solutions. For this purpose, it is well known that natural kaolinite has a small net negative charge, which is attributable to the partial substitution of $Si^{4+}$ ions by $Al^{3+}$ or $Fe^{3+}$ ions (Hai et al., 2015). This permanent negative charge is very beneficial for the surface modification of kaolinite by cationic surfactants, allowing the adsorption of cationic pollutants (e.g., heavy metal ions and cationic dyes) from wastewater. On the other hand, it reduces the affinity of kaolinite towards anions and thus has a negative effect about the adsorption of anionic pollutants by kaolinite.

In short, as it has previously been demonstrated, the capacity of natural kaolinitic clay to adsorb cationic dyes in aqueous solution is much greater than its anionic dye adsorption capacity (Bhattacharyya et al., 2014; El Hassani et al., 2023). Therefore, improving kaolinite's adsorption of anionic azo dyes in aqueous solution remains a major challenge to overcome. One nanomaterial considered in this respect is zinc oxide (ZnO) nanoparticles, a semiconductor metal oxide that exhibits adsorbent and photocatalytic properties (Mahy et al., 2021). Zinc oxide (ZnO) nanoparticles are considered non-toxic, and they have high resistance to chemical and optical corrosion. They also have high catalytic activity and stable chemical properties (Akkari et al., 2018; Mustapha et al., 2020). ZnO is one of the most popular piezoelectric materials (Zhang et al., 2023). Indeed, its elementary cell is made up of a stack of positive and negative charges. It can be seen as an elementary electric dipole with spontaneous polarization. If an external constraint is applied, the positive and negative charges will move, thus creating a piezoelectric polarization (Deschanvres et al., 1992). The difference in electronegativity between the oxygen atom and the zinc atom places zinc oxide on the border between a covalent polar semiconductor and an ionic semiconductor. The disadvantages of ZnO nanoparticles are a low specific surface area, rapid agglomeration and small particle size, which makes recovery from the aqueous phase very difficult. Similarly, the release of ZnO nanoparticles into the environment could pose potential health and environmental risks. Therefore, immobilization of nanoparticles on an appropriate matrix would be a solution to these problems (Akkari et al., 2018; Mustapha et al., 2020).

It has been shown that supported nanoparticles generally have an excellent adsorption capacity compared to unsupported metal oxide nanoparticles (Akkari et al., 2018; Mustapha et al., 2020). Clay is very suitable for this purpose because of its different nanostructures, namely: sheets as found in kaolinite and smectites, fibrous as in sepiolite and palygorskites, or even tubular as in halloysite (Biddeci et al., 2023). It should be noted that the study of clay-semiconductor nanoarchitectures prepared from clay materials is booming and has not yet revealed all its secrets. It has already been demonstrated that the assembly of TiO2 and ZnO nanoparticles with clays of different characteristics takes place mainly on the external surfaces (Ruiz-Hitzky et al., 2019). In addition, Németh et al. (2004) successfully generated ZnO nanoparticles in the interfoliar space of kaolinite following an alkaline hydrolysis of the clay treated with a solution of zinc-cyclohexane butyrate dihydrate in DMSO. Until now, a very limited effort has been made to immobilize ZnO nanoparticles on the surface of a natural kaolinite that has previously undergone physical or chemical activation. The scientific interest of this work is therefore to immobilize the ZnO nanoparticles, which occupy the boundary between a covalent polar semiconductor and an ionic semiconductor, on the external surface of a natural and activated kaolinite originating from southern Cameroon. The aim is to reverse the nature of the surface charge of the composite materials obtained, and to achieve an optimal interaction between the composite materials and the anionic molecules of textile azo dyes in favor of their elimination by adsorption in aqueous solution. Direct Blue 53, Direct Green 1 and Mordant Red 19 will be used as model pollutants.

In Cameroon, the demand for colored loincloth is high, because it is associated with any cultural event (traditional dress, dress designating membership in a clan or tribe, wedding dress, mourning dress and other events, etc.). Water pollution with dye is then an important problem to treat. The development of a water treatment based on a material easily founded in the region is of great interest in such developing countries where the access to expensive technology is not always possible. So, this clay material can be used for the treatment of wastewater mainly loaded with dye and resulting from industrial or artisanal dye baths. This makes it possible to contribute to economic development, viable for the treatment of textile industrial effluents, while promoting sustainable development through the valorization of this local material. The development of this clay material is of interest in the economic and social development of Cameroon, because the transformation of this local raw material will make it possible to achieve foreign exchange savings, create jobs and, consequently, improve the health and living conditions of populations.

## 2. Materials and methods

### 2.1. Clay material and chemicals

The kaolinitic clay ($Al_2Si_2O_5(OH)_4$) used in this work comes from the Kribi deposit in the southern Cameroon region. Deionized water was used as a synthesis solvent, for washing, as well as for purification of clay by extraction of the clay fraction ≤2 μm. Sodium hexametaphosphate ($(Na_6(PO_3)_6)$) was used as a dispersing agent during the purification of clay by extraction of the clay fraction ≤ 2 μm. Hydrochloric acid (HCl, 37%) was used for chemical activation, DMSO was used as a solvent and for intercalation in the interfoliar space of the kaolinite. Absolute ethanol was used to wash KAO-DMSO material, zinc acetate dihydrate ($(Zn(CH_3COO)_2.2H_2O)$) was used as a precursor, sodium hydroxide (NaOH, 0.1 M solution in deionized water) used as a precipitating agent and finally azo textile dyes (Direct Blue 53, Direct Green 1 and Mordant

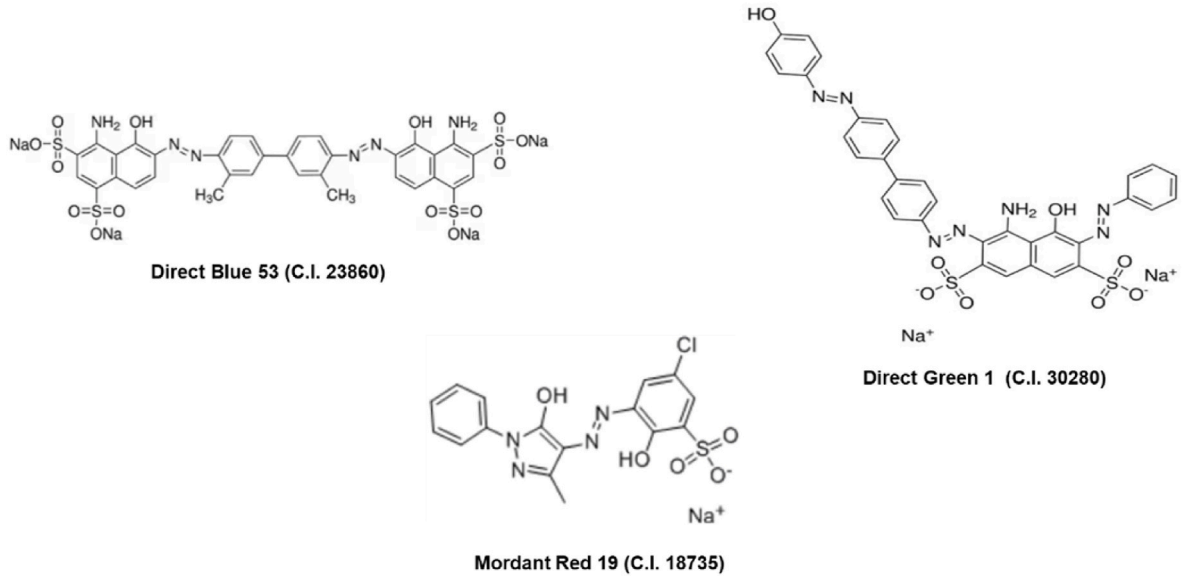


**Fig. 1.** Different types of textile azo dyes used in adsorption studies.

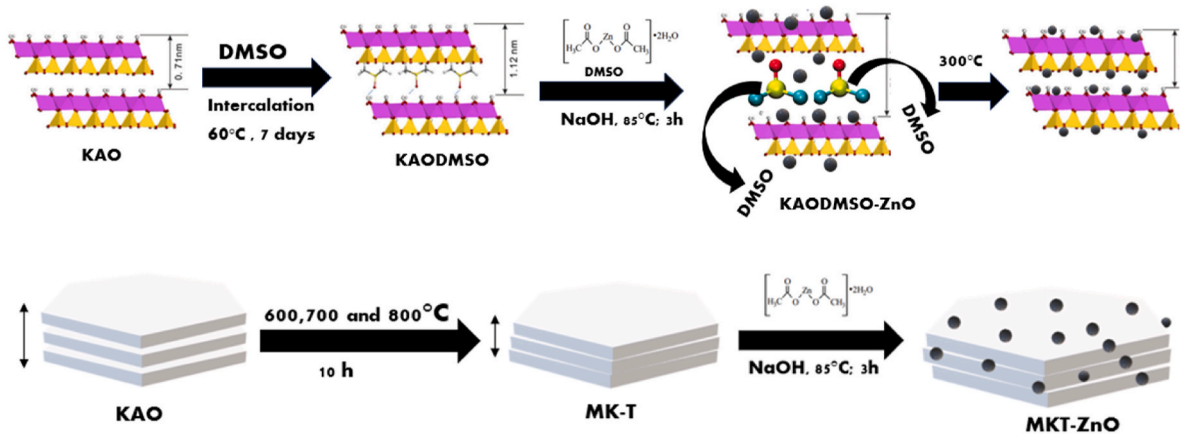


**Fig. 2.** Schematic diagram of the modification with ZnO material.

Red 19), whose molecular structures are illustrated in Fig. 1, were used as received from Sigma-Aldrich.

### 2.2. Activation of clay material by thermal and chemical treatment

The procedures for washing and purification by extraction of the clay fraction ≤2 μm, the heat treatments (600, 700 and 800 °C) that make it possible to obtain metakaolinites (named MK-600, MK-700 and MK-800) and finally the chemical activation by acid treatment (HCl, 6 M, 110 °C, named HCl) of the samples are fully described in (Song et al., 2023) and in Supplementary Materials. The pure kaolinite sample is named KAO.

### 2.3. Intercalation treatment with DMSO

The kaolinite intercalated with DMSO (named KAO-DMSO) was prepared according to the method described by (Gardolinski et al., 2000). Then, a 20 g of kaolinite (clay fraction ≤2 μm, KAO sample) was mixed with 180 mL of DMSO and 20 mL of deionized water. The mixture was subjected to vigorous stirring at 60 °C for 7 days. The sample was then centrifuged (10 min at 14,000 rpm) and further washed with absolute ethanol to remove excess and residual DMSO adsorbed on the surface. The solid residue was subsequently dried at 85 °C for 24 h in an oven under air.

### 2.4. Preparation of ZnO-kaolinite composites

The impregnation ratios of clay materials/zinc acetate dihydrate used are as follows (1:1/2; 1:1). The combination of sol-gel and co-precipitation methods was used for the immobilization of nanoscale ZnO on clay materials. For this purpose, either 2.5 g or 5 g of zinc acetate dihydrate was dissolved in 55 mL of deionized water except in the specific case of nanometric ZnO immobilization on KAO-DMSO where the dissolution of zinc acetate dihydrate took place in 55 mL of DMSO. This is to prevent the DMSO intercalated in the interfoliar spaces of the kaolinite from solubilizing in water. The mixture was stirred vigorously for 10 min at room temperature until the salt dissolved completely. 5 g of clay materials were then added to the previous solution. The mixture was stirred at 85 °C for 1 h while 200 mL of a 0.1 M NaOH solution was added dropwise using a burette so that a milky white precipitate formed. The contents of the reactor are kept stirring at 85 °C for a further 3 h. After cooling to room temperature, the contents were left undisturbed for 12 h. After centrifugation, the solid residue was washed several times with deionized water then dried in an oven at 105 °C for 24 h. The samples modified with ZnO are named with "ZnO". The process of modification with ZnO is represented on Fig. 2.

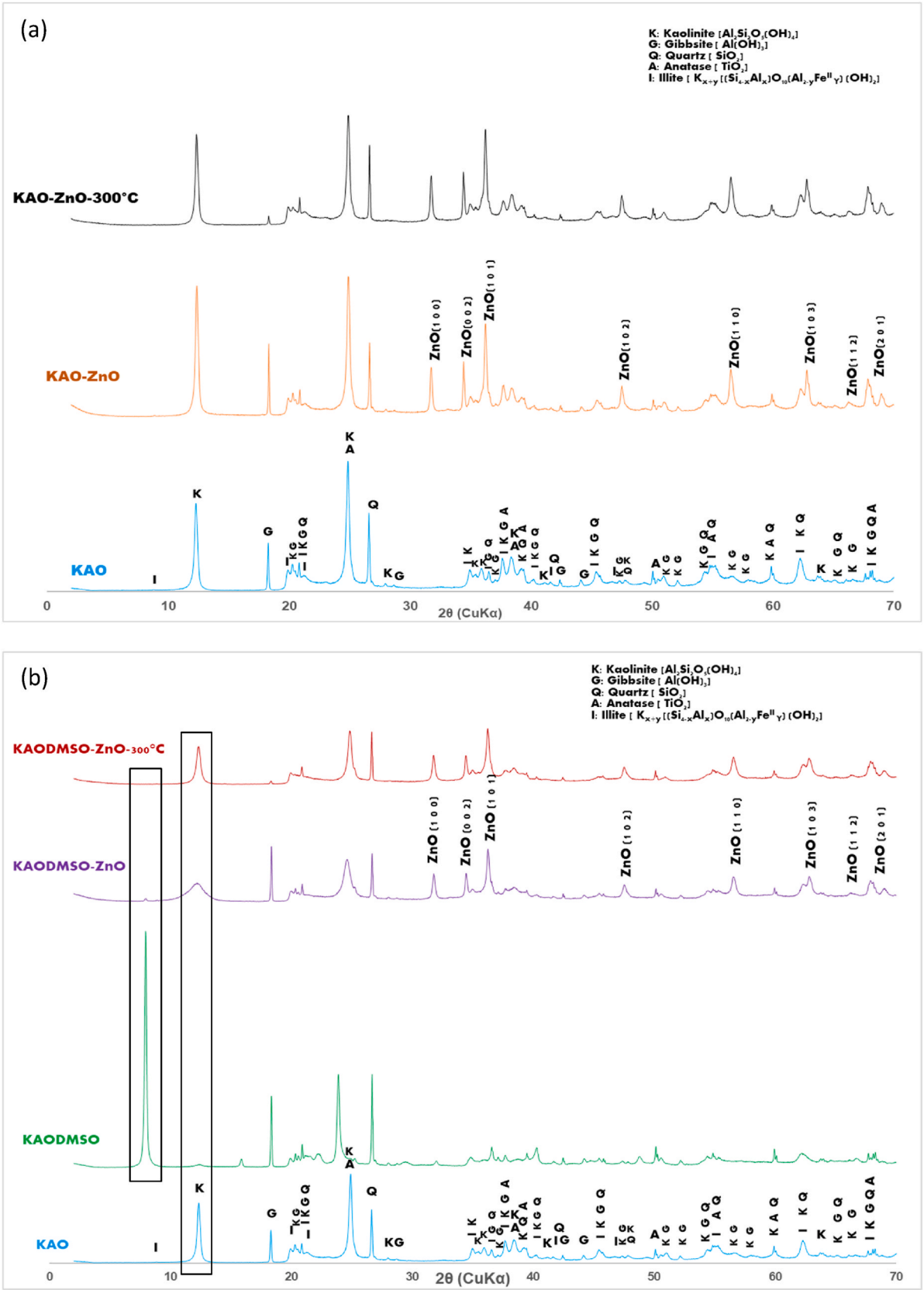


**Fig. 3.** X-Ray diffraction (XRD) patterns of (a): KAO, KAO-ZnO, KAO-ZnO-300 °C, (b): KAO, KAODMSO, KAODMSO-ZnO, KAODMSO-ZnO-300 °C, and (c): KAO, KAOHCl, KAOHCl-ZnO, KAOHCl-ZnO-300 °C samples.

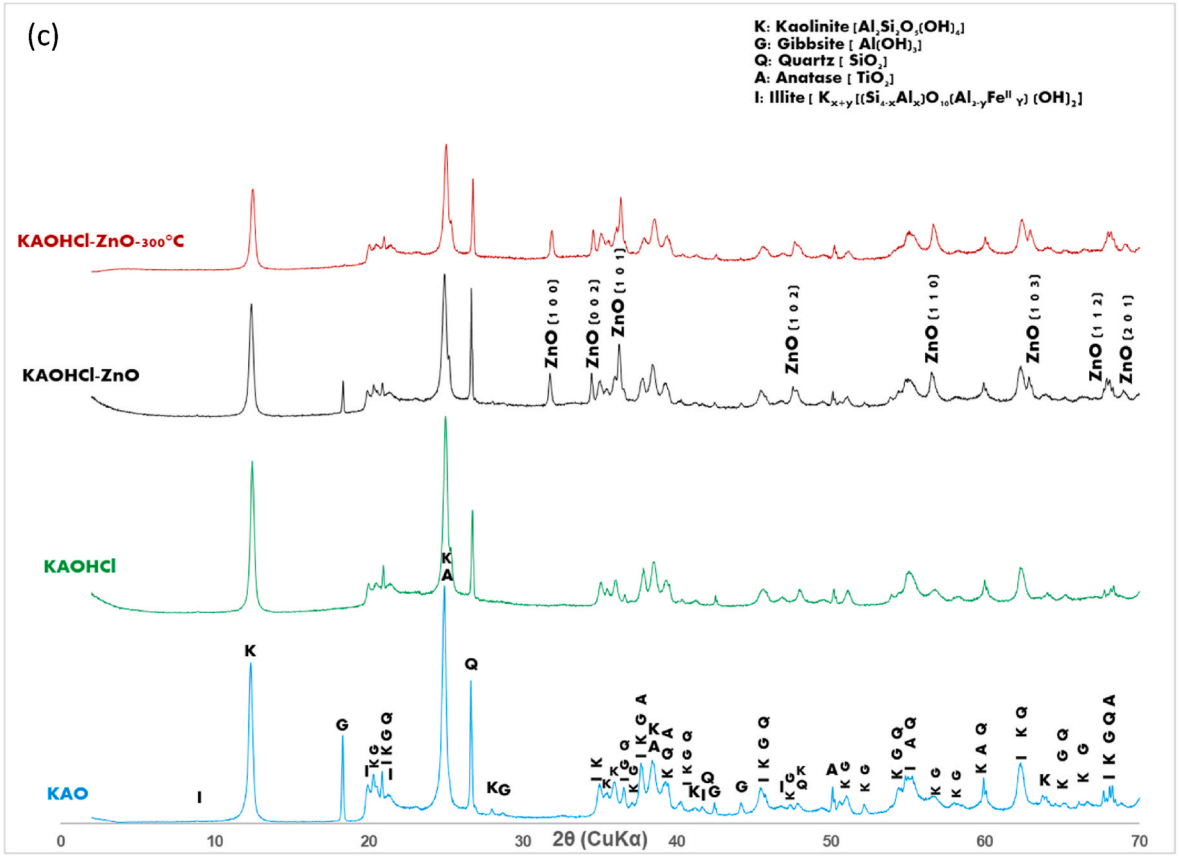


**Fig. 3.** (*continued*).

### 2.5. Material characterizations

The quantity of elements (Al, Si, Ti and Zn) in samples was determined by inductively coupled plasma optical emission spectroscopy (ICP-OES), using a Agilent 5100 instrument. The mineralization is fully described in (Mahy et al., 2016) except that HF was used instead of $HNO_3$.

The crystallographic properties as well as the different crystalline phases observed, through the X-ray diffraction (XRD) patterns, were recorded with a Bruker D8 Twin-Twin powder diffractometer using Cu-Kα radiation, with a step of 0.002° and a scanning speed of 2°/min.

The specific surface area of the materials was determined by nitrogen adsorption-desorption isotherms in a Micromeritics ASAP 2420 multi-sampler volumetric apparatus at −196 °C. Prior to analysis, the samples were outgassed under high vacuum (<2 μm Hg) for 5 h at ambient temperature, followed by 5 h at 105 °C, still under high vacuum.

Scanning electron microscope (SEM) micrographs were obtained using a TESCAN Clara microscope under high vacuum at an accelerating voltage of 15 keV. For sample preparation, in a 10 mL capacity bottle containing 1–2 mg of a powder sample whose particle size is ≤ 2 μm, a few mL of acetone were introduced to obtain a fairly dense suspension. After dispersing everything using ultrasound, the suspensions are deposited in droplets on the glass slide prepared for this purpose. The slide is then placed in an oven under air at 60 °C to evaporate the acetone. The samples are then made conductive by applying a thin layer of gold using a metallizer and finally deposited on a sample port with an adhesive carbon sheet.

Transmission electron microscope (TEM) micrographs were obtained using an FEI TECNAI G2-20 TWIN microscope under an accelerating voltage of 160 kV. For sample preparation, in a 10 mL capacity bottle containing 1–2 mg of a powder sample whose particle size is ≤ 2 μm, a few mL of absolute ethanol were introduced to obtain a suspension. After dispersing the whole using ultrasound, the suspensions are deposited in droplets on a copper grid (Formvar/Carbon 200 Mesh Cu from Agar Scientific).

Zeta potential measurements aimed at evaluating the properties of materials in terms of surface charge were obtained using a Beckman Coulter Delsa Nano C type particle analyzer instrument. In a 20 mL capacity bottle containing 10 mg of a powder sample whose particle size is ≤ 2 μm, 10 mL of Milli-Q water was introduced to obtain a suspension. After dispersing the assembly using ultrasound, the necessary quantity is introduced into the measurement cell after the latter has been purged first with Milli-Q water, then the suspension itself.

### 2.6. Adsorption experiments

The azo anionic textile dyes selected for the adsorption experiments in aqueous solution are Mordant Red 19 (MR19, monoazoic), Direct Blue 53 (DB53, diazoic) and Direct Green 1 (DG1, triazoic). Adsorption experiments in batch mode were carried out by stirring 0.1 g of material with 20 mL of aqueous dye solution at constant pH of 7.4 at 25 °C in different 100 mL brown Duran laboratory flasks. Throughout the adsorption tests, the stirring speed remained constant at 125 rpm. At the end of the predetermined time intervals, the adsorbent was separated from the solution by centrifugation. The residual dye concentrations were obtained by spectrophotometry using the Genesis 10S UV–vis spectrophotometer (Thermo Scientific) at 414 nm, 602 nm and 608 nm, the respective absorption maximums of MR19, DG1 and DB53. Calibration curves were made to set the concentration range of the experiments.

To further evaluate the adsorption kinetics of dyes MR19, DB53 and DG1, the experimental data were analyzed with the plot of the model's pseudo-first order and pseudo-second order kinetics using the following equations (Ho and Mckay, 1999):

**Table 1**
Variation in the size of the immobilized nanometric ZnO crystallites depending on the nature of the matrix.

| Samples | Calcination temperature (°C) | Crystallite size D (nm) |
|---|---|---|
| KAO-ZnO | RT | 38.5 |
| | 300 | 38.7 |
| KAODMSO-ZnO | RT | 32.3 |
| | 300 | 32.6 |
| MK600-ZnO | RT | 26.7 |
| | 300 | 27.5 |
| MK700-ZnO | RT | 28.4 |
| | 300 | 29.1 |
| MK800-ZnO | RT | 15.5 |
| | 300 | 19.4 |
| KAOHCl-ZnO | RT | 49.2 |
| | 300 | 48.3 |
| MK800HCl–ZnO | RT | 30.9 |
| | 300 | 31.2 |

RT: room temperature (18 °C).

**Table 2**
Sample chemical composition by inductively coupled plasma-optical emission spectroscopy (ICP-OES).

| Samples | Ratio clay/zinc acetate dihydrate | Amount (in wt%) | | | |
|---|---|---|---|---|---|
| | | *Al* | *Si* | *Ti* | *Zn* |
| KAO | – | 19.50 | 19.70 | 1.10 | 0.01 |
| KAO-ZnO | (1:1) | 15.80 | 15.90 | 0.93 | 12.90 |
| | (1:1/2) | 17.10 | 17.00 | 0.99 | 11.40 |
| KAODMSO-ZnO | (1:1) | 14.90 | 15.00 | 0.45 | 13.90 |
| | (1:1/2) | 16.50 | 16.90 | 0.60 | 12.80 |
| MK600-ZnO | (1:1) | 18.80 | 18.50 | 1.08 | 11.20 |
| | (1:1/2) | 18.30 | 18.60 | 1.10 | 11.00 |
| MK700-ZnO | (1:1) | 18.30 | 18.50 | 1.08 | 10.70 |
| | (1:1/2) | 18.70 | 18.80 | 1.11 | 10.90 |
| MK800 | – | 22.20 | 22.50 | 1.33 | 0.02 |
| MK800-ZnO | (1:1) | 18.50 | 18.60 | 1.10 | 11.50 |
| | (1:1/2) | 19.00 | 19.10 | 1.09 | 10.80 |

$$\ln(q_e - q_t) = ln\ q_e - k_1 t \quad (1)$$

$$\frac{t}{q_t} = \frac{1}{k_2 q_e^2} + \frac{t}{q_e} \quad (2)$$

where $q_t$ (mg/g) and $q_e$ (mg/g) are the quantities of azo dyes adsorbed respectively at time $t$ (min) and at equilibrium; $k_1$ ($min^{-1}$) and $k_2$ (g $mg^{-1}$ $min^{-1}$) are the rate constants of the pseudo-first and pseudo-second order kinetics, respectively.

## 3. Results and discussion

### 3.1. Crystalline composition

The crystal structure, the pure kaolinite phase (KAO) and those amorphized at 600, 700 and 800 °C (MK-600, MK-700 and MK-800) as well as the acid-treated samples (KAO-HCl, and MK-800-HCl) under reflux conditions were studied and the results are presented in (Song et al., 2023).

Fig. 3 and S1 to S4 present the X-ray diffractograms of kaolinite intercalated with DMSO and those of the KAO-ZnO, KAODMSO-ZnO, MK-ZnO, KAOHCl-ZnO and MK800HCl–ZnO nanocomposites. These diffractograms show the presence of ZnO nanoparticles immobilized on the matrix whatever the composite, through the three main reflection peaks of ZnO having values of 2θ between 30 and 40° (Mahy et al., 2021, 2022; Chérif et al., 2023; Misra et al., 2018; Staroń, 2023). These diffractograms highlight the presence of eight reflection peaks characteristic of ZnO in the wurtzite crystalline phase with the space symmetry group P63mc (JCPDS 36-1451). These reflection peaks recorded at 2θ = 31.82°, 34.44°, 36.33°, 47.66°, 56.72°, 62.85°, 66.55° and 69.11° correspond respectively to the crystallographic planes (100), (002), (101), (102), (110), (103), (112) and (201) of ZnO in this crystalline phase (Mahy et al., 2021, 2022; Chérif et al., 2023; Misra et al., 2018; Staroń, 2023). It was noted that the calcination of the nanocomposites (Fig. 3 and S1 to S4) at 300 °C for 1 h caused an increase in the intensity of the peaks. This increase in peak intensity is stronger with the increasing calcination temperature of the kaolinite to obtain metakaolinite (Figs. S1–S4). This increase in the intensity of the reflection

**Table 3**
Variation of the zeta potential at pH 7.2–7.5 at 25 °C of the nanocomposites depending on the nature of the matrix and the treatment.

| Samples | Impregnation ratio (clay material/zinc acetate dihydrate) | Solvent and synthesis temperature | Calcination temperature (°C) | Zeta potential (mV) |
|---|---|---|---|---|
| Pure ZnO | – | – | 300 | 20.13 ± 1.1 |
| KAO | – | – | RT | −37.58 ± 1.6 |
| KAO-ZnO | 1:1/2 | $H_2O$; 85 °C | RT | −11.15 ± 0.9 |
| | | | 300 | −14.82 ± 1.1 |
| KAO-ZnO | 1:1 | $H_2O$; 85 °C | RT | +16.79 ± 1.3 |
| KAODMSO | | DMSO; $H_2O$; 60 °C | RT | −26.97 ± 1.8 |
| KAODMSO-ZnO (1) | 1:1/2 | DMSO; 85 °C | RT | −5.54 ± 1.0 |
| | | | 300 | −13.23 ± 1.2 |
| KAODMSO-ZnO (1) | 1:1 | DMSO; 85 °C | RT | +30.10 ± 1.1 |
| KAODMSO-ZnO (2) | 1:1 | $H_2O$; 85 °C | RT | +19.60 ± 2.0 |
| KAOHCl | | HCl, 6 M; 110 °C | RT | −25.83 ± 1.7 |
| KAOHCl-ZnO | 1:1/2 | $H_2O$; 85 °C | RT | −20.45 ± 2.1 |
| | | | 300 | −19.97 ± 1.5 |
| MK600 | | | RT | −31.24 ± 1.9 |
| MK600-ZnO | 1:1/2 | $H_2O$; 85 °C | RT | +30.97 ± 2.6 |
| | | | 300 | +27.94 ± 2.4 |
| MK600-ZnO | 1:1 | $H_2O$; 85 °C | RT | +32.02 ± 1.8 |
| MK700 | | | RT | −29.74 ± 2.3 |
| MK700-ZnO | 1:1/2 | $H_2O$; 85 °C | RT | +29.30 ± 1.4 |
| | | | 300 | +25.27 ± 2.7 |
| MK700-ZnO | 1:1 | $H_2O$; 85 °C | RT | +36.04 ± 2.1 |
| MK800 | | | RT | −24.49 ± 2.3 |
| MK800-ZnO | 1:1/2 | $H_2O$; 85 °C | RT | +29.96 ± 1.3 |
| | | | 300 | +23.75 ± 1.8 |
| MK800-ZnO | 1:1 | $H_2O$; 85 °C | RT | +34.11 ± 2.4 |
| MK800HCl | | HCl, 6 M; 110 °C | RT | −21.50 ± 1.0 |
| MK800HCl–ZnO | 1:1/2 | $H_2O$; 85 °C | RT | −23.87 ± 1.7 |
| | | | 300 | −26.57 ± 1.9 |
| MK800HCl–ZnO | 1:1 | $H_2O$; 85 °C | RT | −22.09 ± 1.5 |

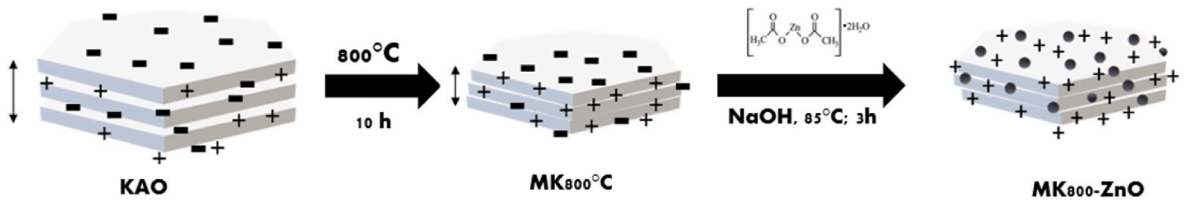


**Fig. 4.** Schematic representation of the evolution of the clay's charge density after each treatment.

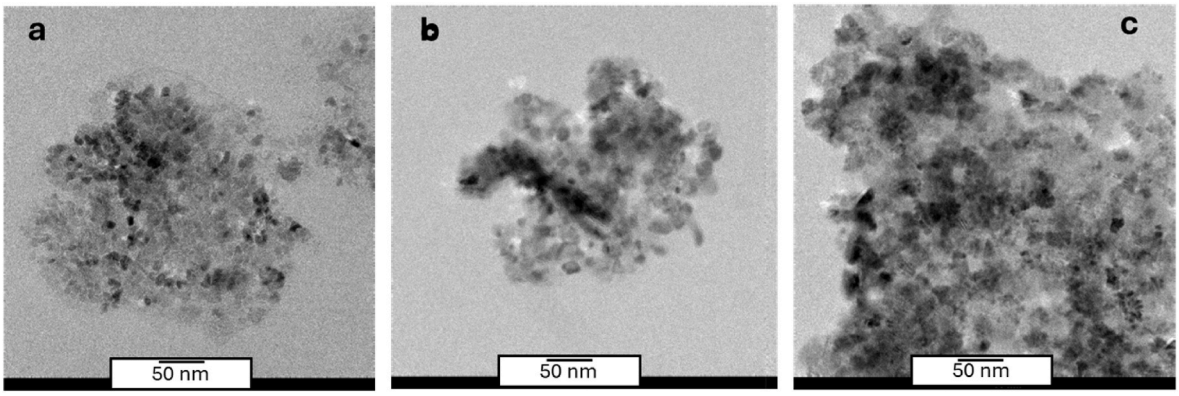


**Fig. 5.** TEM images of KAO-ZnO (a); KAODMSO-ZnO (b) and MK800-ZnO (c).

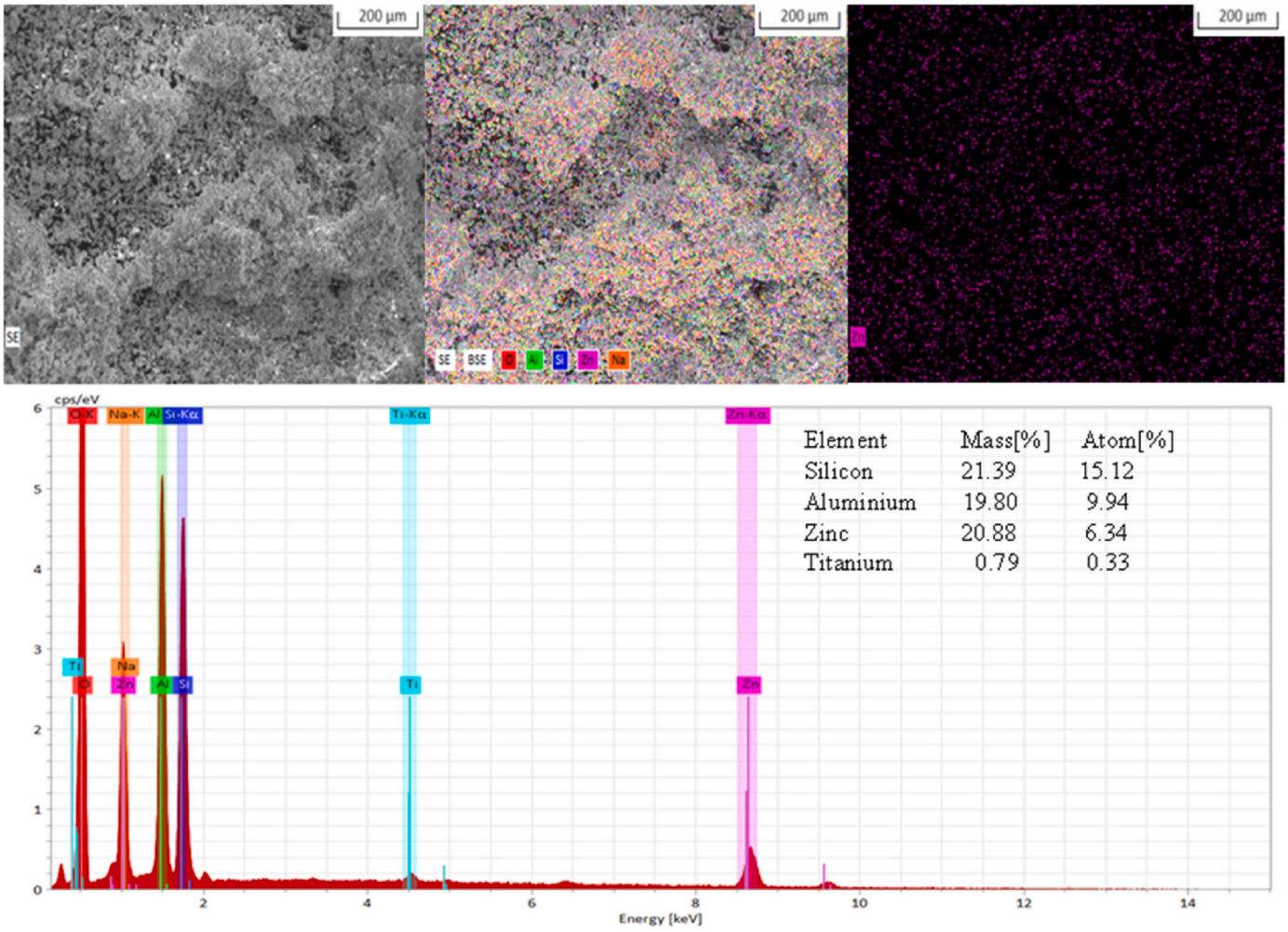


**Fig. 6.** SEM-EDX picture and mapping for KAO-ZnO(1:1/2) sample.

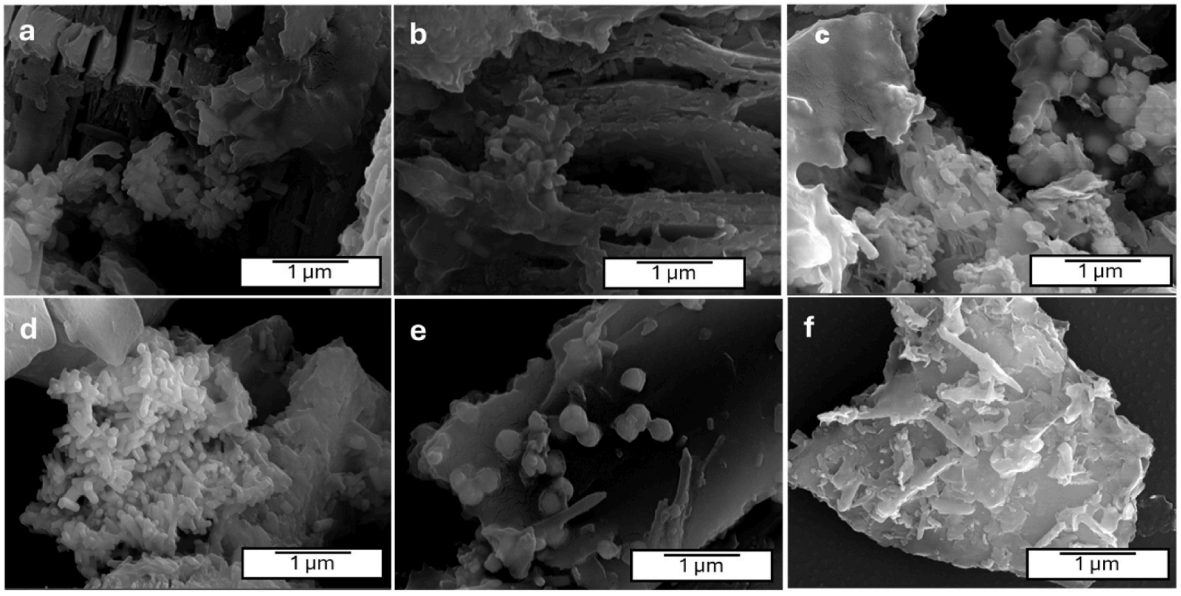


**Fig. 7.** Scanning electron microscope images of (a) KAODMSO, (b) KAO-ZnO, (c) KAODMSO-ZnO, (d) KAO-ZnO300 °C, (e) KAODMSO-ZnO300 °C and (f) MK800-ZnO.

**Table 4**
Textural properties of all samples.

| Sample | $S_{BET}$ ($m^2$/g) ±5 | $S_{meso}$ ($m^2$/g) ±5 | $S_{micro}$ ($m^2$/g) ±5 | $V_T$ ($cm^3$/g) ±0.01 | $V_{meso}$ ($cm^3$/g) ±0.01 | $V_{micro}$ ($cm^3$/g) ±0.01 |
|---|---|---|---|---|---|---|
| KAO | 20 | 15 | 5 | 0.09 | 0.08 | 0.01 |
| KAO-ZnO(1:1/2) | 15 | 10 | 5 | 0.05 | 0.04 | 0.01 |
| KAO-ZnO(1:1) | 13 | 08 | 5 | 0.03 | 0.02 | 0.01 |
| KAODMSO | 30 | 25 | 5 | 0.1 | 0.08 | 0.02 |
| KAODMSOZnO (1)(1:1/2) | 20 | 15 | 5 | 0.09 | 0.08 | 0.01 |
| KAODMSO-ZnO (1)(1:1) | 17 | 12 | 5 | 0.05 | 0.04 | 0.01 |
| KAODMSO-ZnO (2)(1:1) | 19 | 14 | 5 | 0.06 | 0.05 | 0.01 |
| KAOHCl | 95 | 80 | 15 | 0.27 | 0.22 | 0.05 |
| KAOHCl-ZnO (1:1) | 65 | 50 | 15 | 0.20 | 0.18 | 0.02 |
| MK600 | 30 | 25 | 5 | 0.1 | 0.08 | 0.02 |
| MK600-ZnO(1:1/2) | 18 | 13 | 5 | 0.05 | 0.04 | 0.01 |
| MK600-ZnO(1:1) | 16 | 11 | 5 | 0.05 | 0.04 | 0.01 |
| MK700 | 30 | 25 | 5 | 0.1 | 0.08 | 0.02 |
| MK700-ZnO(1:1/2) | 18 | 13 | 5 | 0.05 | 0.04 | 0.01 |
| MK700-ZnO(1:1) | 15 | 10 | 5 | 0.05 | 0.04 | 0.01 |
| MK800 | 25 | 20 | 5 | 0.1 | 0.08 | 0.02 |
| MK800-ZnO(1:1/2) | 15 | 10 | 5 | 0.05 | 0.04 | 0.01 |
| MK800-ZnO(1:1) | 13 | 08 | 5 | 0.03 | 0.02 | 0.01 |
| MK800HCl | 315 | 175 | 140 | 0.33 | 0.2 | 0.13 |
| MK800HCl–ZnO (1:1) | 240 | 140 | 100 | 0.32 | 0.2 | 0.12 |

peaks with temperature would be linked either to an increase in the crystallinity of the immobilized nanometric ZnO, or to the growth of ZnO crystallites. Other authors who carried out a study on the crystallite size and crystallinity of ZnO with increasing calcination temperature came to the same conclusions (Ashraf et al., 2015; Golsheikh et al., 2018).

It is known that when kaolinite is calcined above 450–500 °C, dehydroxylation occurs to give metakaolinite. This transformation involves the loss of structural water and the collapse of the crystal lattice, which is accompanied by reorganization of the structure. Only part of the $AlO_6$ octahedra is preserved; the majority being transformed into much more reactive tetra- and penta-coordinated units (Belver et al., 2002; Lenarda et al., 2007). Furthermore, the breakage or weakening of the strong hydrogen bonds between adjacent layers (interfoliar spaces) of the kaolinite (Song et al., 2023; Tang et al., 2017) was obtained by intercalation of DMSO (a very polar organic molecule) into these spaces. To this end, the X-ray diffraction diagram (Fig. 3b) shows a complete shift in the reflection peak characteristic of kaolinite from $2\theta = 12.4°$ to $2\theta = 7.9°$. This is a shift in the reflection peak (001) of kaolinite from 0.71 nm to 1.13 nm, thus confirming the formation of the KAO-DMSO complex. The increase in basal spacing of 0.41 nm is consistent with ordered monolayer intercalation of DMSO in kaolinite layers (Leal et al., 2021; Mbey et al., 2013). However, it should be noted that this intercalation is not total because the kaolinite reflection peak remains at $2\theta = 12.4°$ (Fig. 3b, KAO-DMSO). The immobilization of nanometric ZnO in the interlamellar space of the kaolinite sheets would be achieved by expulsion of the intercalated DMSO. This is due to the strong polarity difference between DMSO and ZnO (Marin et al., 2009; V Panasiuk et al., 2014). In addition, the difference in electronegativity between the oxygen atom and that of zinc places ZnO at the border between a covalent polar semiconductor and an ionic semiconductor (Rasmidi et al., 2021).

However, in the case of this kaolinite from southern Cameroon, the immobilization of nanometric ZnO in the interfoliar space occurred to a small extent. To this end, we observe a partial return of the reflection peak characteristic of low-intensity broadband kaolinite at $2\theta = 12.4°$ (Fig. 3b, KAODMSO-ZnO). (Németh et al., 2004) obtained the same result with German kaolinite from the municipality of Zettlitz. The presence of the reflection peak of very low intensity which remains at $2\theta = 7.9°$ (Fig. 3b, KAODMSO) after immobilization of the ZnO in the interfoliar space of this kaolinite is proof that all the DMSO intercalated beforehand was not expelled. This is further confirmed with its almost total disappearance after the calcination of the composite (KAODMSO-ZnO, Fig. 3b) at 300 °C (temperature higher than the boiling point of DMSO) for 1 h. We also observe the complete return of the reflection peak characteristic of kaolinite at $2\theta = 12.4°$, of low intensity and a slightly wider band compared to that of the original kaolinite (Fig. 3b). The absence of the reflection peak characteristic of one of the compounds $Al_2O_3$, $SiO_2$, or (Zn–Al–Si–O; Zn–Ti–Al–O; Zn–Ti–Si–O) in all these diffractograms eliminate the possibility of alloy formation. Other

**Table 5**
Kinetic parameters for the adsorption of the 3 different dyes on kaolinitic clay and composite materials.

| Adsorbent | Zeta potential (mv) | Dyes | $C_0$(mg/L) | $RR_{max}$(%) | $q_{e,exp}$ (mg/g) | Pseudo-first order-model | | | Pseudo-second order-model | | |
|---|---|---|---|---|---|---|---|---|---|---|---|
| | | | | | | $K_1$ ($min^{-1}$) | $q_{e,cal}$ (mg/g) | $R^2$ | $K_2$ ($g\ mg^{-1}\ min^{-1}$) | $q_{e,cal}$ (mg/g) | $R^2$ |
| MK800-ZnO(1:1) | **+34.11** | | 100 | 99 | 19.85 | 0.0198 | 0.03 | 0.0357 | 2.5301 | 19.88 | 1 |
| MK800-ZnO(1:1/2) | **+29.96** | | 100 | 98 | 19.72 | 0.7240 | 45.01 | 1 | 0.3188 | 19.80 | 1 |
| KAODMSO-ZnO(1)(1:1) | **+30.10** | **MR19** | 100 | 99 | 19.81 | 1.2108 | 707.11 | 1 | 0.2400 | 19.92 | 0.9999 |
| KAODMSO-ZnO(2)(1:1) | **+19.60** | | 100 | 88 | 17.66 | 0.0768 | 0.95 | 0.9956 | 0.2217 | 17.76 | 1 |
| KAO-ZnO(1:1) | **+16.79** | | 100 | 78 | 15.51 | 0.0741 | 0.72 | 0.9858 | 0.2882 | 15.58 | 1 |
| KAODMSO-ZnO(1)(1:1/2) | **−5.54** | | 100 | 46 | 09.29 | 0.0630 | 0.30 | 0.9959 | 0.5457 | 09.32 | 1 |
| KAO-ZnO(1:1/2) | **−11.15** | | 100 | 35 | 07.06 | 0.0850 | 0.32 | 0.8300 | 0.7336 | 07.09 | 1 |
| KAO Adsorbent | **−37.58** | | 100 | 17 | 3.44 | 0.0663 | 0.59 | 0.8782 | 0.2268 | 3.52 | 0.9997 |
| MK800-ZnO(1:1) | **+34.11** | | 100 | 99 | 19.99 | 0.5678 | 4.79 | 1 | 1.3889 | 20.00 | 1 |
| MK800-ZnO(1:1/2) | **+29.96** | | 100 | 99 | 19.98 | 0.0922 | 0.12 | 0.3348 | 0.4788 | 20.04 | 0.9999 |
| KAODMSO-ZnO(1)(1:1) | **+30.10** | **DB53** | 100 | 99 | 19.98 | 0.0988 | 0.18 | 0.6838 | 0.3831 | 20.04 | 1 |
| KAODMSO-ZnO(2)(1:1) | **+19.60** | | 100 | 92 | 19.96 | 0.0499 | 0.77 | 0.9737 | 0.1767 | 18.69 | 0.9999 |
| KAO-ZnO(1:1) | **+16.79** | | 100 | 83 | 19.91 | 0.0749 | 0.07 | 0.8178 | 0.2232 | 20.00 | 1 |
| KAODMSO-ZnO(1)(1:1/2) | **−5.54** | | 100 | 66 | 13.32 | 0.0510 | 0.69 | 0.8781 | 0.1988 | 13.40 | 1 |
| KAO-ZnO(1:1/2) | **−11.15** | | 100 | 43 | 09.45 | 0.1898 | 2.92 | 1 | 0.2037 | 09.56 | 0.9999 |
| KAO Adsorbent | **−37.58** | | 100 | 14 | 02.79 | 0.0494 | 0.82 | 0.9007 | 0.1316 | 02.88 | 0.9999 |
| MK800-ZnO(1:1) | **+34.11** | | 100 | 97 | 19.35 | 0.8004 | 18.26 | 1 | 1.2679 | 19.38 | 1 |
| MK800-ZnO(1:1/2) | **+29.96** | | 100 | 96 | 19.25 | 0.1000 | 0.47 | 0.7764 | 0.4810 | 19.27 | 1 |
| KAODMSO-ZnO(1)(1:1) | **+30.10** | | 100 | 95 | 18.99 | 0.0993 | 0.36 | 0.5630 | 0.3281 | 19.05 | 1 |
| KAODMSO-ZnO(2)(1:1) | **+19.60** | **DG1** | 100 | 84 | 16.70 | 0.1399 | 2.08 | 0.9579 | 0.1893 | 16.81 | 1 |
| KAO-ZnO(1:1) | **+16.79** | | 100 | 71 | 14.29 | 0.1540 | 0.68 | 1 | 0.6584 | 14.33 | 1 |
| KAODMSO-ZnO(1)(1:1/2) | **−5.54** | | 100 | 60 | 11.99 | 0.2286 | 2.43 | 0.8682 | 0.2466 | 12.08 | 0.9999 |
| KAO-ZnO(1:1/2) | **−11.15** | | 100 | 33 | 6.58 | 0.2163 | 1.44 | 0.9821 | 0.4698 | 6.63 | 1 |
| KAO | **−37.58** | | 100 | 11 | 2.26 | 0.0458 | 0.39 | 0.9328 | 0.3321 | 2.31 | 0.9994 |

authors (Misra et al., 2018) have reached the same conclusion. The XRD data were used to evaluate the ZnO crystallite sizes of the nanocomposites. The Scherrer equation illustrated by relation (3) was used to calculate the average diameter of these crystallites.

$$D = \frac{k\lambda}{\beta\, Cos\, \theta} \tag{3}$$

where $D$ is the crystallite size in nanometers, $k$ is a constant equal to 0.9, $\theta$ is the angle at which the diffraction intensity is maximum, while $\beta$ is the full width at half maximum. The average diameter of ZnO crystallites in various nanocomposites, obtained from a clay material/zinc acetate dihydrate impregnation ratio (1:1/2), is calculated using the Scherrer formula and the results are presented in Table 1.

The variation in the size of the crystallites and their growth with temperature is a function of the matrix on which the nanometric ZnO is immobilized. Metakaolinites are ideal matrices for the immobilization of ZnO whose crystallites are smaller.

### 3.2. Chemical composition

Table 2 presents the results of the elemental analyses by ICP-OES. These made it possible to determine the evolution and content in wt% of 4 essential elements (Al, Si, Ti and Zn) in the clay fraction (KAO), the metakaolinite obtained at 800 °C and some nanocomposites (KAO-ZnO, KAODMSO-ZnO, MK600-ZnO, MK700-ZnO and MK800-ZnO) obtained from the impregnation ratios of clay materials/zinc acetate dihydrate (1:1/2) and (1:1).

From this analysis, the clay fraction (KAO) contains silicon and aluminum at 19.70% and 19.50% respectively. Titanium has a mass percentage equal to 1.10%, while zinc is present with a very low content (0.01%). From these results we can therefore assume that quartz and aluminosilicates are predominant in this clay fraction. The Si/Al mass ratio is equal to 1.01, which indicates a high kaolinite content (Khalifa et al., 2019; Mkaouar et al., 2019). The heat treatment of this kaolinite at 800 °C caused an increase of 2.8% in the silicon and 2.7% in aluminum content, and only 0.23% of that of titanium. This increase in the silicon and aluminum content is essentially due to the collapse of the crystal lattice, by the transformation of part of the $AlO_6$ octahedra into much more reactive tetra and pentacoordinate units (Song et al., 2023; Belver et al., 2002). However, this increase did not affect the Si/Al mass ratio which remains constant due to the conservation of the material. Kenne Diffo et al. (Kenne Diffo et al., 2015) arrived at the same conclusion in their study of the effect of the calcination rate of kaolin on the properties of geopolymers based on metakaolin. However, whatever the nanocomposite, we note for an impregnation ratio of (1:1/2), that the mass of Zn in KAO-ZnO, KAODMSO-ZnO and MK800-ZnO is respectively 11.40%, 12.80% and 10.80%. The difference, not really being significant (<2%) from one matrix to another, suggests that whatever nanocomposite and in the same ratio, the mass of immobilized nanometric ZnO is approximately the same. KAODMSO-ZnO had a slightly higher Zn content (12.8%). This slightly high quantity of ZnO immobilized on KAODMSO is explained by the immobilization of nanometric ZnO in the interfoliar spaces of the kaolinite in addition to the surface. To this end, the treatment of kaolinite with DMSO (very polar solvent) caused the breakage or weakening of the strong hydrogen bonds between the neighboring layers of the kaolinite (Song et al., 2023; Tang et al., 2017). This was not the case with KAO and MK where the immobilization of nanometric ZnO was found only on the surface. In the case of metakaolinites, this situation is explained by the fact that the calcination of

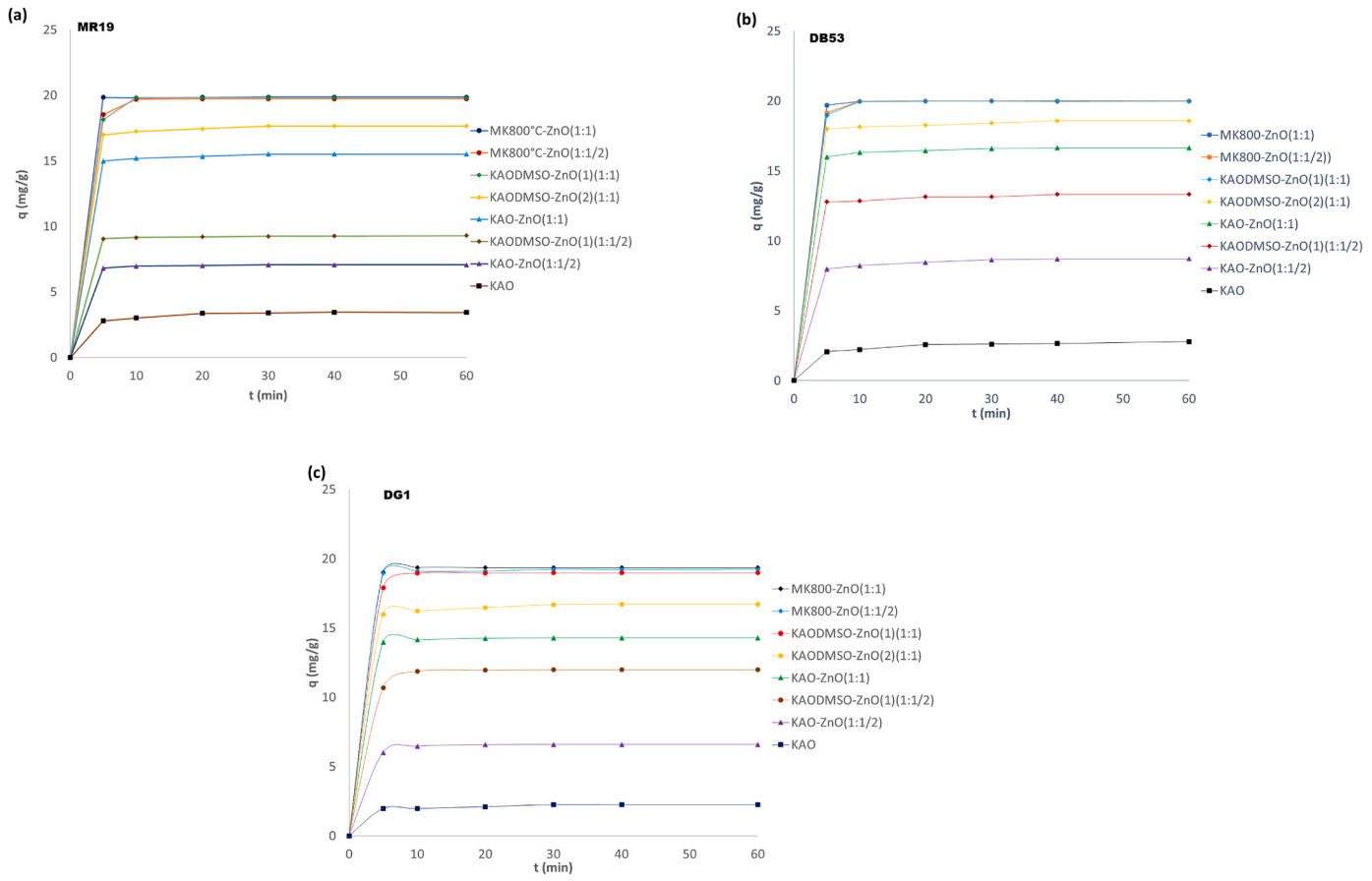


**Fig. 8.** Effect of contact time on the removal of dyes by kaolinitic clay and composite materials: with dyes (a) MR19, (b) DB53 and (c) DG1. Conditions: $C_0 = 100$ mg/L; $V_0 = 20$ mL; m = 0.1 g; pH = 7.4; T = 298 K.

kaolinite above 400 or even 500 °C, as in the case of treatment with DMSO, causes the breakdown of the hydrogen bonds between the adjacent kaolinite layers. This causes the collapse of the crystal lattice, which is accompanied by a thinning of the layers due to the reduction of the interfoliar space (Song et al., 2023; Ptáček et al., 2010). The increase in the clay material/zinc acetate dihydrate impregnation ratio (1:1) contributed to the increase in the Zn content to only 1.5% in KAO-ZnO, 1.1% in KAODMSO-ZnO and 0.7% in MK800-ZnO. This slight increase in the mass percentage of Zn with the impregnation ratio (1:1) simply reflects the surfaces of the different matrices having reached saturation by the immobilization of nanometric ZnO on them. This surface saturation is quickly reached in the MK, followed by the KAO and finally by the KAODMSO.

### 3.3. Zeta potential of samples in suspension

The zeta potential is established on the surface of a nanoparticle in suspension or in solution. It is a very important interfacial property making it possible to evaluate the intensity of the electrostatic repulsion/attraction that exists between the different nanoparticles (Kamble et al., 2022). It also indicates the affinity and, under certain conditions, makes it possible to predict the capacity of nanoparticles to retain other chemical species present in a solution. It therefore represents the effective net surface charge of nanoparticles and colloids under these conditions (Henderson et al., 2008).

Table 3 presents the variation in the zeta potential, obtained at pH 7.2–7.5 at 25 °C, of the nanocomposites depending on the nature of the matrix and the type of treatment undergone. It clearly appears that KAO (clay fraction ≤2 μm) has a zeta potential value equal to −37.58 mV. This value is in agreement with those obtained for the measurement of the zeta potential of other kaolinites in the literature in the pH range 7.0–7.5 (Lu et al., 2021; Yukselen-Aksoy and Kaya, 2011). This negative charge is obtained through the contribution of two major processes, namely the imperfections of the crystal lattice of this kaolinite through its average degree of structural order reported by (Song et al., 2023). These cause an isomorphic substitution inside the network. For this purpose, in the tetrahedral layer a $Si^{4+}$ can be replaced by an $Al^{3+}$ and in the octahedral layer in the same way an $Al^{3+}$ can be replaced by a $Mg^{2+}$, $Fe^{2+}$, … (Silva et al., 2017; Chen et al., 2022). In a given cell, the electropositive elements see the sum of their valences compensated by the $O^{2-}$ ions, the replacement of the ions by ions of lower positive valence results in a charge deficit which will appear in the form of a negative charge carried by the network (Cuisset, 1980). However, it should be noted in this case that the sign and magnitude of the reticular charge are independent of the characteristics of the aqueous phase. Also, many natural colloids contain surface functional groups that can ionize. In the case of kaolinites, these are the silanol (-Si-OH) and aluminol (-Al-OH) groups which can then ionize, producing negative primary charges depending on the pH conditions of the medium (Ahmed, 1966). On the other hand, the heat treatment at 600, 700 or even 800 °C of kaolinite from southern Cameroon, having made it possible to obtain MK600, MK700 and MK800, caused a significant increase in the zeta potential despite the negative values obtained. The same is true for the treatment of kaolinite with DMSO. It was noted that this increase in zeta potential becomes more and more significant as the calcination temperature of the kaolinite increases (from −37.58 mV for KAO to −24.49 mV for MK800, Table 3), because, as mentioned above, the treatment (thermal or DMSO intercalation) causes the rupture or weakening of the strong hydrogen bonds between the adjacent kaolinite layers. High temperature heat treatment also contributes to this increase in this sense

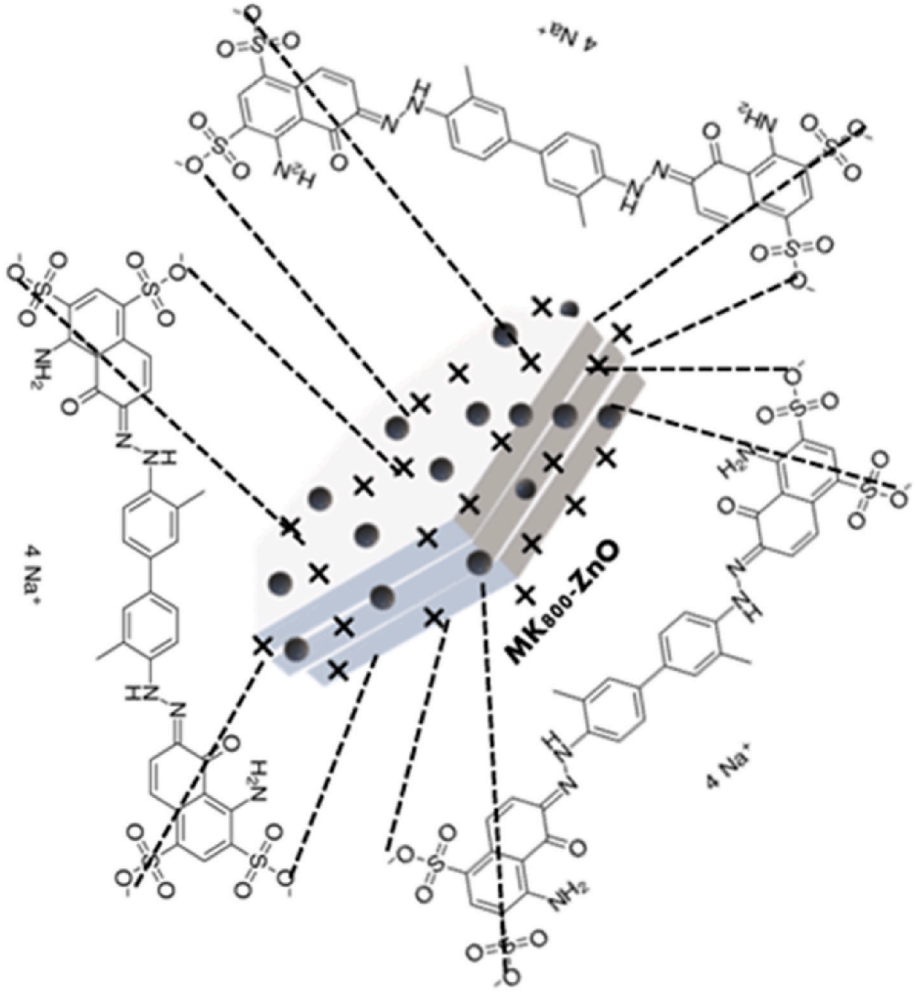


**Fig. 9.** Electrostatic interaction between the anionic molecules of DB53 and the surface charges of MK800-ZnO. The dark dots represent ZnO nanoparticles.

by the collapse of the crystal lattice. This is accompanied by a reorganization of its structure caused by the dehydroxylation of kaolinite under these conditions. Furthermore, based on the authors' previous work, hot acid treatment is necessary to accelerate the interface reactions of clay minerals (Jia et al., 2019). For KAO and MK800, hot acid did not greatly change the situation, despite a slight increase in the value of the zeta potential, which was more significant in KAOHCl than in MK800HCl (from −25.83 to −21.50 mV, Table 3). We could have expected a different result since kaolinite's greater resistance to acid leaching compared to metakaolinites has been proven in other studies (Song et al., 2023; Belver et al., 2002).

The immobilization of the semiconductor, nanometric ZnO, on the surface of the kaolinite and whether the kaolinite had undergone physical or chemical activation provided very interesting results for an impregnation ratio of clay material/zinc acetate dihydrate (1:1/2). An abrupt increase is observed across the positive and high values of the recorded zeta potential, except in the case of KAO-ZnO, KAODMSO, KAOHCl-ZnO and MK800HCl–ZnO where they remained negative. However, it must be noted that the increase and sudden variation in the zeta potential after immobilization of the semiconductor depend on the nature of the matrix; in other words, the type of activation or treatment undergone by the kaolinite. For this purpose, the zeta potential is +30.97 mV; +29.30 mV and +29.96 mV; these values corresponding respectively to MK600-ZnO, MK700-ZnO and MK800-ZnO. The following zeta potential was found for KAODMSO-ZnO(1), whose value is −5.54 mV. Finally comes those of the KAO-ZnO, KAOHCl-ZnO, MK800HCl–ZnO nanocomposites with respective values of −11.15 mV, −20.45 mV and −22.94 mV. ZnO is found on the border between a covalent polar semiconductor and an ionic semiconductor (Rasmidi et al., 2021); due to this atypical feature, immobilization on the surface of the different matrices (KAO, KAODMSO, KAOHCl, MK600, MK700, MK800 and MK800HCl) causes the modification of the nature and of the density of the charges at the basal and side surfaces (Fig. 4). This modification is very intense in the case of metakaolinites and not sufficient, at this impregnation ratio, to reverse the situation at the level of the other matrices (KAO, KAODMSO, KAOHCl and MK800HCl), despite the fact that the quantity of immobilized nanometric ZnO, is substantially the same according to chemical analyses (Table 2). However, the calcination of the previous nanocomposites at 300 °C for 1 h resulted in the increased growth and crystallinity of the ZnO crystallites immobilized in the metakaolinites. On the other hand, it has the opposite effect of reducing the potential values of the nanocomposites by increasing the density of negative charges on their surfaces.

However, for the clay material/zinc acetate dihydrate impregnation ratio (1:1), we note an increase in the zeta potential values compared to those recorded for the clay material/zinc acetate dihydrate impregnation ratio (1:1/2). As before, this variation differs from one matrix to another. Thus, the zeta potential values of the MK600-ZnO, MK700-ZnO and MK800-ZnO nanocomposites are respectively +32.02 mV; +36.04 mV and +34.11 mV. Compared to the previous clay material/zinc acetate dihydrate impregnation ratio (1:1/2), they correspond respectively to an increase of: 3%, 23% and 13%. Similarly, the zeta potential values of the KAO-ZnO, KAODMSO-ZnO(1) and KAODMSO-ZnO(2) nanocomposites are respectively +16.79 mV; +30.10 mV and +19.60 mV.

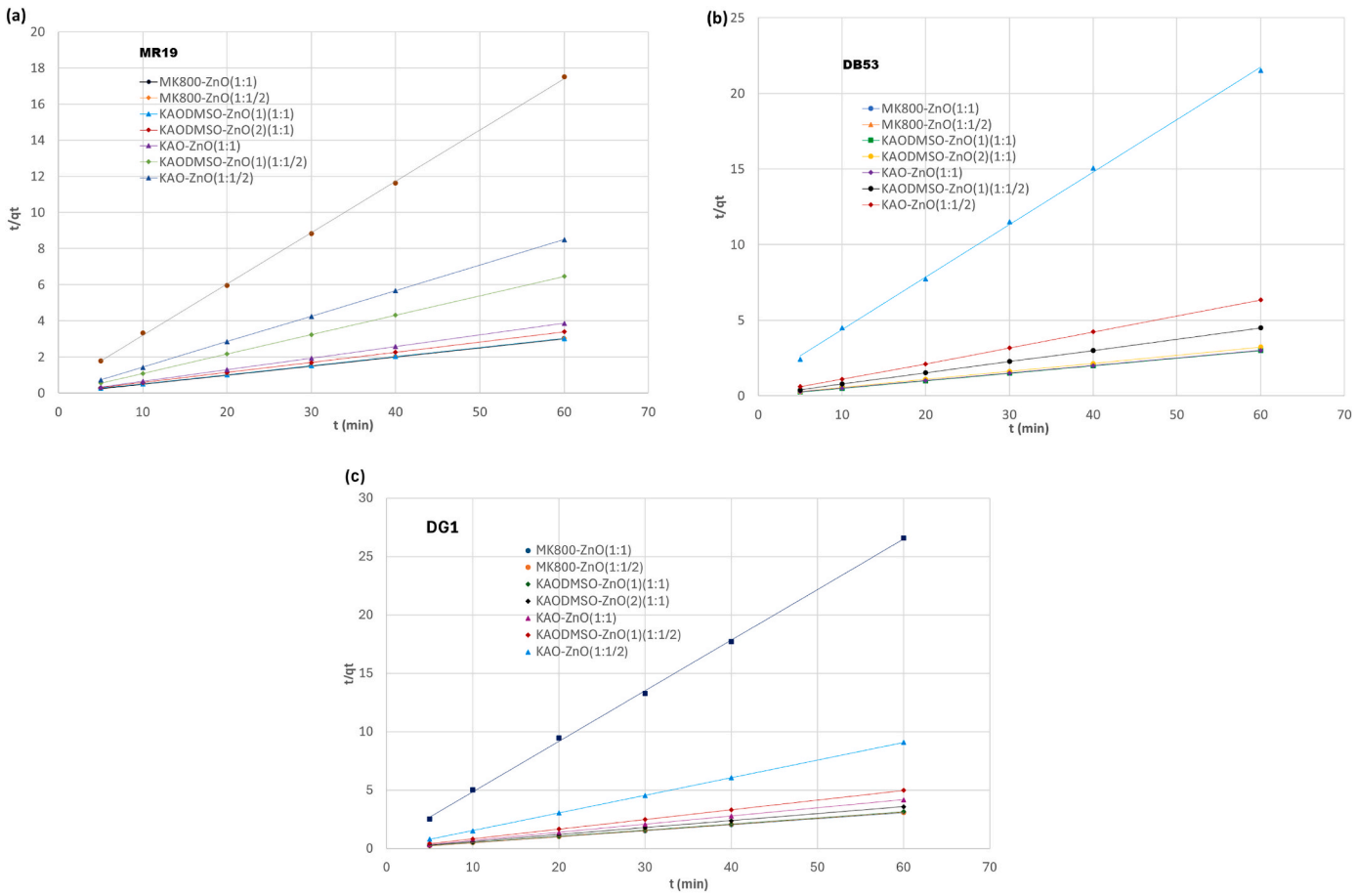


**Fig. 10.** Pseudo-second-order adsorption kinetics of (a) MR19, (b) DB53 and (c) DG1 on kaolinitic clay and composite materials.

Compared with the initial impregnation ratio of clay material/zinc acetate dihydrate (1:1/2), these values are equivalent to an increase of 250%, 643% and 453% respectively. The 190% difference in the increase in the zeta potential value between KAODMSO-ZnO(1) and KAODMSO-ZnO(2) comes from the synthetic solvent. The KAODMSO matrix was dispersed in an aqueous solution of zinc acetate dihydrate. The water therefore caused the dissolution of part of the DMSO molecules intercalated in the interfoliar spaces of the kaolinite. This was not the case with KAODMSO-ZnO(1) or the KAODMSO matrix, it was instead dispersed in DMSO having previously dissolved the zinc acetate dihydrate.

The small variation in the zeta potential, in the MK600-ZnO, MK700-ZnO and MK800-ZnO nanocomposites after the impregnation ratio increased to (1:1), can be explained by the saturation of the charge density at level of the basal surfaces and the lateral surfaces. Chemical analyses also provide confirmation with the low variation in the Zn content in MK800-ZnO obtained either for an impregnation ratio (1:1/2) or (1:1). All the same, it should be noted that metakaolinites (MK600, MK700 and MK800) remain ideal and appropriate matrices for immobilization of nanometric ZnO given the zeta potential values recorded at low impregnation ratios. This fundamental difference in the evolution of the surface charge of the metakaolinites observed after the immobilization of the nanometric ZnO would probably be linked to the heat treatment of the kaolinite. When kaolinite is calcined above 450–500 °C, dehydroxylation occurs to give metakaolinite. This transformation involves the loss of structural water accompanied by a reorganization of its structure. Only a part of the $AlO_6$ octahedra is preserved while the majority is transformed into much more reactive tetra- and penta-coordinated units (Song et al., 2023; Belver et al., 2002). These tetra- and penta-coordinated units would be the determining factor, responsible for the rapid inversion of the surface charge, and by extension the exponential increase in the zeta potential after the immobilization of the nanometric ZnO on these metakaolinites. This hypothesis is again confirmed, because the values of the zeta potentials of MK800HCl and MK800HCl–ZnO remained in the same order of magnitude (Table 3). This observation finds an explanation in the fact that these tetra- and penta-coordinate units are much more reactive, that is to say more sensitive to hot acid leaching, than the $AlO_6$ octahedra.

### 3.4. Morphology of samples

#### 3.4.1. TEM micrographs of distributions of ZnO nanoparticles in composite materials

The TEM micrographs of certain nanocomposites at the same magnifications are presented in Fig. 5. Each sample examined contains crystalline ZnO with size in the range of that determined by the Scherrer method from the XRD diffractograms (by measuring approximatively 20 nanoparticles). Whatever the sample, ZnO aggregates are observed in an order of magnitude hundreds nanometers (Fig. 5a, b, c). On the other hand, we observe that these aggregates are composed of small uniform spheres. The two materials (clay and ZnO) can be distinguished: the sheets in lighter material and the ZnO in the darker sphere. It is to remind that crystalline ZnO and clay were detected by XRD in the hybrid materials (see section 3.1). These indicate successful coverage and deposition of spherical ZnO nanoparticles, heterogeneously distributed on the surfaces of the KAO, KAODMSO and MK800 (Fig. 5). These spherical ZnO nanoparticles are between 19 and 40 nm in size. As we reported for the X-ray diffractograms of the composites, we observe that the size of the ZnO crystallites vary from one matrix to another.

The presence of the homogeneous ZnO particles repartition on clay is

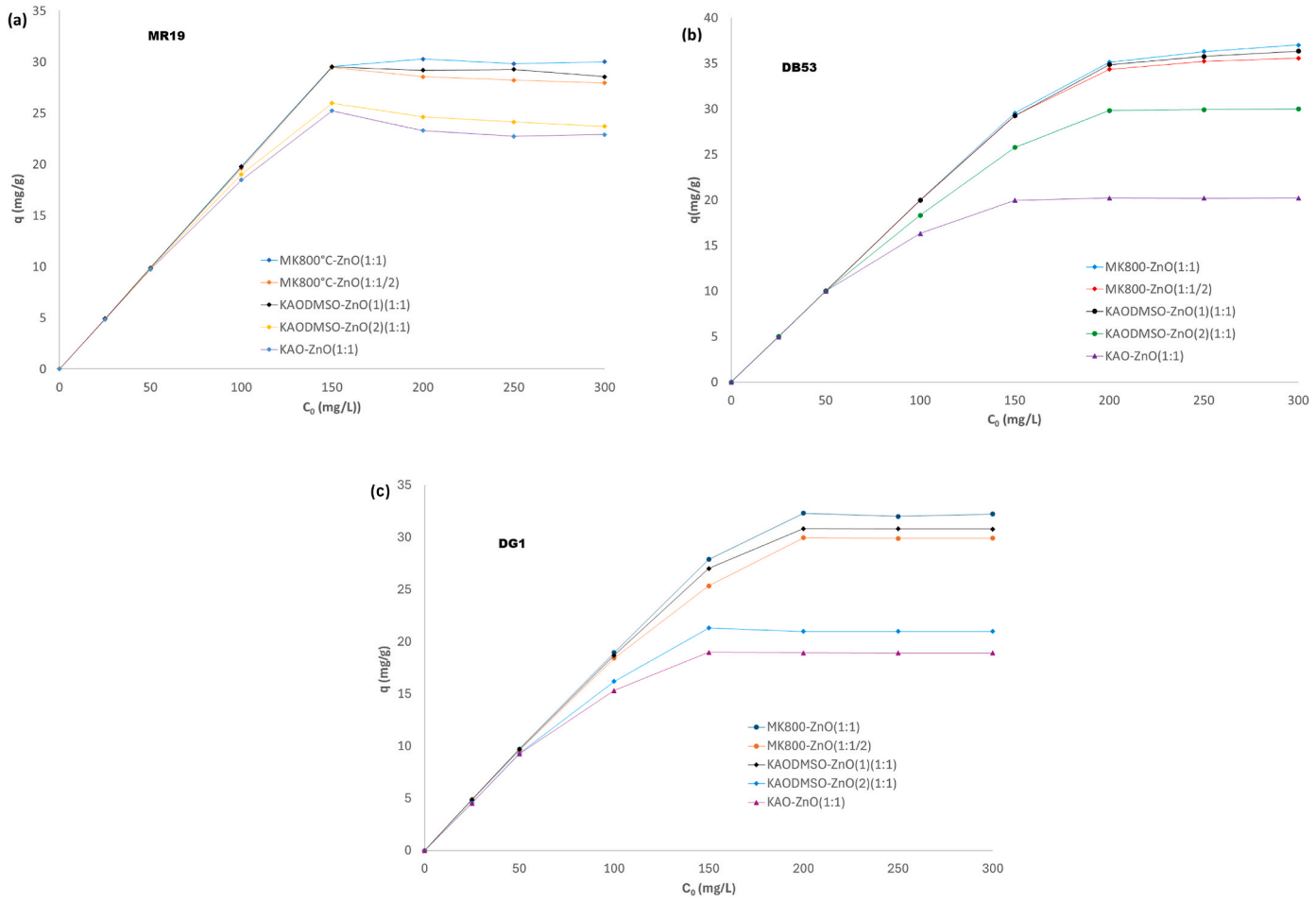


**Fig. 11.** Effect of initial dye concentration on the removal of (a) MR19, (b) DB53 and (c) DG1 by 5 composite materials. Conditions: $V_0 = 20$ mL; m = 0.1 g; pH = 7.4; T = 298 K.

confirmed by EDX analysis (Fig. 6, For KAO-ZnO(1:1/2) sample and Fig. S5 for KAODMSO-ZnO(1:1/2) and KAODMSO-ZnO(1:1)). The EDX analysis (Fig. 6) shows a successful coverage and deposition of ZnO nanoparticles through a homogeneous distribution of Zn on the different surfaces of the KAO particles (Fig. 6).

### 3.4.2. *SEM micrographs of composite materials*

Fig. 7a, b, c, d, e and f present the SEM micrographs of KAODMSO, KAO-ZnO, KAODMSO-ZnO, KAO-ZnO300 °C, KAODMSO-ZnO300 °C and MK800-ZnO samples respectively. These micrographs confirm the heterogeneous texture of the different matrices on which the nanometric ZnO was immobilized. We can therefore observe the typically two-dimensional morphology of kaolinite (Song et al., 2023; Tang et al., 2017) (Fig. 7a). EDX analyzes also provide confirmation since they qualitatively highlight the presence of Zn on the surface of the kaolinite particles (Fig. 6).

## 3.5. *Texture of the samples*

The BET surface areas and pore volumes of all materials are listed in Table 4. Natural kaolinitic clay, the basis for the synthesis of all composites, has a specific surface area of 20 $m^2$/g. After physical activation by heat treatment (600, 700 and 800 °C) or chemical activation by treatment with DMSO, we see that the specific surface area increases from 20 to 30 $m^2$/g, despite the dehydroxylation obtained and the breakage of the strong hydrogen bonds present between adjacent layers. This corresponds to a slight increase in the total porous volume from 0.09 to 0.1 $cm^3$/g. However, the acid treatment of KAO and MK800 under hot reflux conditions causes a significant modification of the texture as detailed in (Song et al., 2023). For this purpose, we note that the specific surface area of kaolinite increases from 20 to 95 $m^2$/g and that of MK800 from 25 to 315 $m^2$/g. Furthermore, it should be emphasized that this increase in specific surface area is accompanied by a significant development of microporosity and mesoporosity (Table 4). However, the textural analysis of the composite materials provides confirmation of the immobilization of the ZnO nanoparticles on the different surfaces (basal and lateral) of the kaolinite particles, as well as those having undergone either physical or chemical activation. This can be explained with particular regard to the reduction in specific surface areas (Table 4). (Hai et al., 2015) reached the same conclusion with the immobilization of $TiO_2$ nanoparticles on a natural and activated Chinese kaolinite. However, it was noted that this reduction in the specific surface area after immobilization of the ZnO nanoparticles is increasingly strong in composites made from kaolinite, having previously undergone physical or chemical activation.

## 3.6. *Adsorption of dyes by composite materials*

### 3.6.1. *Influence of contact time*

Table 5 gives the results of the study of the influence of the contact time for the adsorption of 20 mL of each of the dye solutions (MR19, DB53 and DG1) with a concentration 100 mg/L at pH 7.4 with 0.1 g of each of the adsorbent matrices (MK800-ZnO(1:1), MK800-ZnO(1:1/2), KAODMSO-ZnO(1)(1:1), KAODMSO-ZnO(2)(1:1), KAO-ZnO(1:1), KAODMSO-ZnO(1)(1:1/2), KAO-ZnO(1:1/2) and KAO). The quantity of dye adsorbed as a function of time is represented by Fig. 8a, b and c.

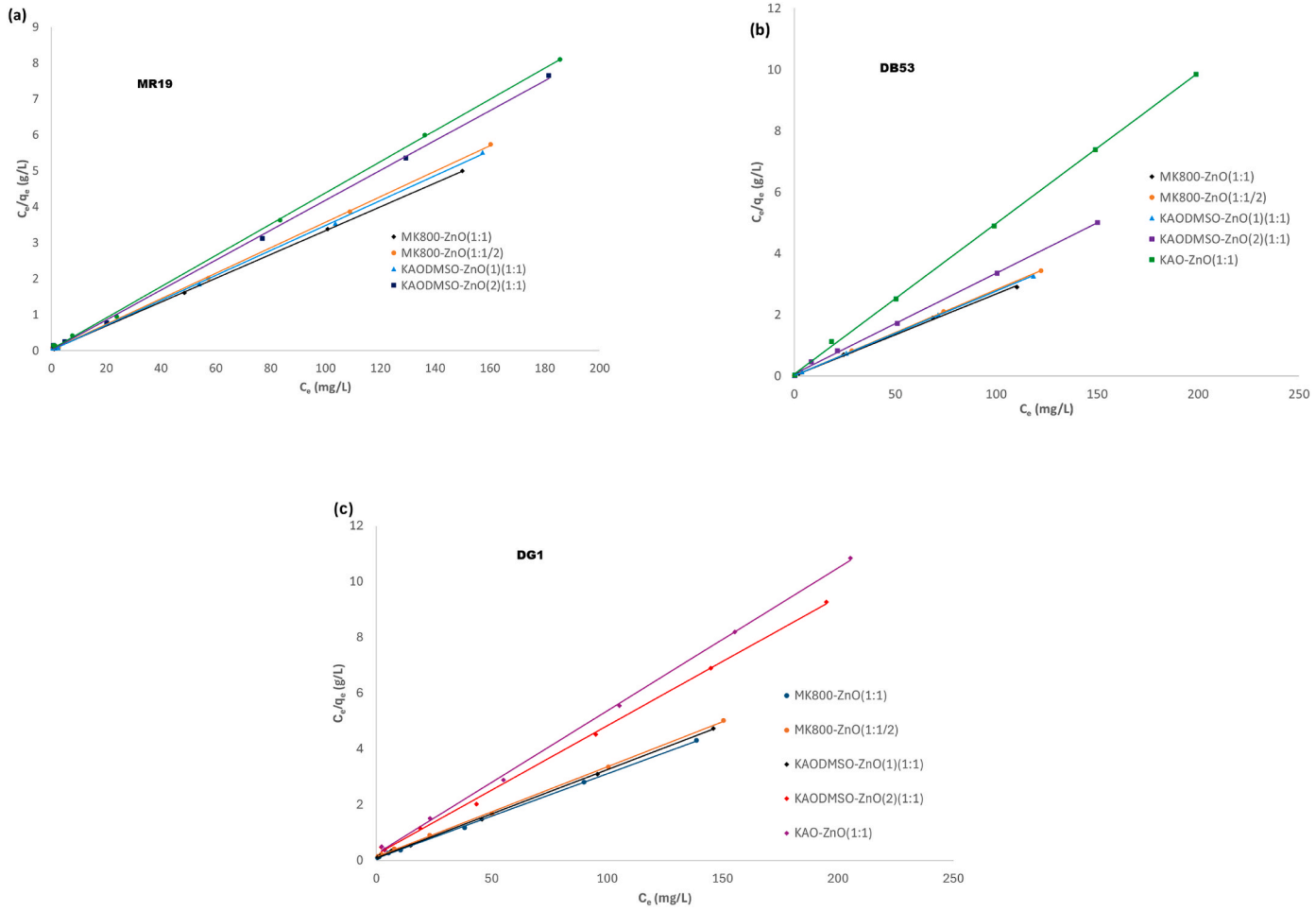


**Fig. 12.** Langmuir model isotherm with (a) MR19, (b) DB53 and (c) DG1 for MK800-ZnO(1:1), MK800-ZnO(1:1/2), KAODMSO-ZnO(1)(1:1), KAODMSO-ZnO(2)(1:1) and KAO-ZnO(1:1).

**Table 6**
Langmuir and Freundlich isotherm parameters of MK800-ZnO(1:1), MK800-ZnO(1:1/2), KAODMSO-ZnO(1)(1:1), KAODMSO-ZnO(2)(1:1) and KAO-ZnO(1:1).

| Adsorbent | Dyes | Langmuir model | | | | Freundlich model | | |
|---|---|---|---|---|---|---|---|---|
| | | $q_m$ (mg/g) | $K_L$ (L/mg) | $R_L$ | $R^2$ | $K_F$ | n | $R^2$ |
| MK800-ZnO(1:1) | | 30.2 | 1.1696 | 0.0168 | 0.9998 | 12.56 | 4.71 | 0.5748 |
| MK800-ZnO(1:1/2) | | 28.2 | 1.3460 | 0.0146 | 0.9998 | 11.66 | 4.64 | 0.5977 |
| KAODMSO-ZnO(1)(1:1) | | 28.9 | 1.6321 | 0.0121 | 0.9996 | 12.21 | 4.76 | 0.5785 |
| KAODMSO-ZnO(2)(1:1) | **MR19** | 24.0 | 1.5639 | 0.0126 | 0.9993 | 8.77 | 4.22 | 0.7298 |
| KAO-ZnO(1:1) | | 23.0 | 0.9156 | 0.0214 | 0.9995 | 8.07 | 4.12 | 0.7706 |
| Adsorbent | | | | | | | | |
| MK800-ZnO(1:1) | | 37.7 | 1.4480 | 0.0136 | 0.9993 | 18.02 | 5.26 | 0.7214 |
| MK800-ZnO(1:1/2) | | 35.6 | 1.9514 | 0.0101 | 0.9999 | 16.74 | 5.18 | 0.7138 |
| KAODMSO-ZnO(1)(1:1) | **DB53** | 36.4 | 1.7188 | 0.0115 | 0.9999 | 16.64 | 4.94 | 0.7414 |
| KAODMSO-ZnO(2)(1:1) | | 30.5 | 0.4391 | 0.0436 | 0.9989 | 20.19 | 4.46 | 0.9094 |
| KAO-ZnO(1:1) | | 20.4 | 0.6945 | 0.0280 | 0.9996 | 9.53 | 6.21 | 0.8561 |
| Adsorbent | | | | | | | | |
| MK800-ZnO(1:1) | | 33.0 | 0.3890 | 0.0489 | 0.9997 | 8.81 | 3.12 | 0.8570 |
| MK800-ZnO(1:1/2) | | 30.9 | 0.2351 | 0.0784 | 0.9995 | 7.09 | 2.96 | 0.9062 |
| KAODMSO-ZnO(1)(1:1) | **DG1** | 31.6 | 0.3238 | 0.0582 | 0.9996 | 8.01 | 3.08 | 0.8778 |
| KAODMSO-ZnO(2)(1:1) | | 21.7 | 0.1990 | 0.0913 | 0.9989 | 5.24 | 3.30 | 0.8284 |
| KAO-ZnO(1:1) | | 19.5 | 0.2092 | 0.0873 | 0.9993 | 5.19 | 3.62 | 0.8322 |

Whatever the dye and the adsorbent matrix considered, the adsorption dynamics between 0 and 60 min clearly show that the kinetics are divided into three phases: first, a linear and rapid increase in the quantity of adsorbed dye is observed during the first 5 min. To this end, we therefore record retention rates (RR (%)) of (MR19: 97%, 93%, 90%, 85%, 75%, 45%, 34%, 14%); (DB53: 98%, 96%, 95%, 90%, 80%, 64%, 40%, 10%); (DG1: 95%, 94%, 89%, 80%, 70%, 53%, 30%, 10%) corresponding respectively to MK800-ZnO(1:1), MK800-ZnO(1:1/2), KAODMSO-ZnO(1)(1:1), KAODMSO-ZnO(2)(1:1), KAO-ZnO(1:1), KAODMSO-ZnO(1)(1:1/2), KAO-ZnO (1:1/2) and KAO samples. This is followed by a transition regime which also extends over 5 min, and finally a plateau reflecting an equilibrium reached after 10 min.

From the above and with regard to the RRmax (%) recorded (Table 5), it is clear that the efficiency of adsorption strongly depends on the zeta potential of the material. For this purpose, the higher the zeta potential is towards positive values, the better the adsorption capacities of the nanocomposites.

However, this surface phenomenon, by which anionic azo dye molecules attach to the solid surface of nanocomposites, is potentially governed by physisorption forces. This can possibly be of three different origins: electrostatic interactions between the sulfonate groups ($SO_3^-$) of the anionic dye molecules (MR19, DB53, DG1) and the positive surface charges of the nanocomposites (see Fig. 9); the polar forces resulting from the presence of an electric field in the micropores of the nanocomposites; and finally from the hydrogen bonds that can be established between the hydroxyl (-OH) and amine (-$NH_2$) groups of the dye molecules (MR19, DB53, DG1), and the silanol (-SiOH) and aluminol (-AlOH) groups of certain nanocomposites. Consequently, kaolinite's capability to eliminate anionic azo dye molecules can be considerably improved by modifying it by physical or chemical activation followed by immobilization of ZnO nanoparticles on the surface.

### 3.6.2. Adsorption kinetics

To further evaluate the adsorption kinetics of dyes MR19, DB53 and DG1, the experimental data were analyzed with the plot of the model's pseudo-first order (Figure S6a, b and c) and pseudo-second order (Fig. 10a, b and c) kinetics using equations (1) and (2).

The values of the rate constants ($k_1$ and $k_2$), the calculated equilibrium adsorption capacities ($q_{e,\,cal}$) and the linear correlation coefficients ($R^2$) are listed in Table 5. In most cases, the pseudo-first-order kinetic model showed a lower value of ($R^2$). Furthermore, the values of $q_{e,\,cal}$ obtained from this model do not agree with those of experimental $q_e$, which suggests that the kinetics of adsorption of dyes on the different materials does not follow this model. On the other hand, the values of ($R^2$) of the pseudo-second order kinetic model are all greater than 0.99, and the values of $q_{e,\,cal}$ are close to the experimental values $q_e$. The plot $t/q_t$ versus $t$ is a straight line in all cases (Fig. 10a, b and c). The linear plot suggests a good fit of the experimental data with the pseudo-second-order kinetic model, indicating that this model is more appropriate to describe the adsorption of MR19, DB53 and DG1 on the different matrices.

### 3.6.3. Adsorption isotherms

The adsorption isotherms of MR19, DB53 and DG1 of 5 nanocomposites: MK800-ZnO(1:1), MK800-ZnO(1:1/2), KAODMSO-ZnO(1)(1:1), KAODMSO-ZnO (2)(1:1) and KAO-ZnO(1:1) are shown in Fig. 11a, b and c.

Regardless of the material, initially the adsorption capacities of the three dyes increase linearly between 0 and 150 mg/L, then reach a plateau at 200 mg/L which reflects the saturation of the available active sites and beyond which they do not evolve anymore. Several adsorption isotherm models have been developed to study the adsorption phenomenon. Among these, the Langmuir and Freundlich isothermal models are the most used because they have proven useful in translating a number of adsorption processes. However, the underlying assumptions of the two models are quite different. The Langmuir isothermal model assumes that adsorption takes place on specific homogeneous active sites, of the same energy within the adsorbent. They can only complex a single molecule of the solute (monolayer adsorption) and there are no interactions between the adsorbed molecules (Páez et al., 2012). The Freundlich model is based on adsorption on a heterogeneous surface (Páez et al., 2012). In the present study, we used both models to analyze the experimental data. The linearized Langmuir equation can be translated as follows:

$$\frac{C_e}{q_e} = \frac{1}{K_L q_m} + \frac{C_e}{q_m} \tag{4}$$

where $C_e$ (mg/L) is the equilibrium dye concentration, $q_e$ (mg/g) is the equilibrium adsorption capacity, $K_L$ (L/mg) is the Langmuir equilibrium constant and $q_m$ (mg/g) is the maximum adsorption capacity. The values of $K_L$ and $q_m$ can be determined from the linear plot $C_e/q_e$ versus $C_e$. The equilibrium parameter $R_L$, which describes the feasibility of adsorption, is defined as follows:

$$R_L = \frac{1}{1 + K_L C_0} \tag{5}$$

where $K_L$ (L/mg) is the Langmuir equilibrium constant and $C_0$ (mg/L) is the initial dye concentration. Adsorption is more favorable as ($R_L \to 0$) and more unfavorable as ($R_L \to 1$).

The Langmuir isotherms are represented in Fig. 12.

Likewise, the Freundlich equation can be translated as follows:

$$\ln q_e = \ln K_F + \frac{1}{n} \ln C_e \tag{6}$$

where $q_e$ (mg/g) is the equilibrium adsorption capacity, $K_F$ is the Freundlich adsorption equilibrium constant, $n$ is a Freundlich intensity factor and $C_e$ (mg/L) is the concentration of the dye at equilibrium.

The Freundlich isotherms are represented in Fig. S7.

Table 6 lists the values of all Langmuir and Freundlich adsorption isotherm parameters corresponding to the adsorption of MR19, DB53 and DG1 on the nanocomposites MK800-ZnO(1:1), MK800-ZnO(1:1/2), KAODMSO-ZnO(1)(1:1), KAODMSO-ZnO(2)(1:1) and KAO-ZnO(1:1). The linear correlation coefficients ($R^2$) of the Langmuir adsorption isotherms are all greater than 0.99. While those of the Freundlich isotherm vary between 0.5748 and 0.9094, indicating that the adsorption data best fit the Langmuir adsorption isotherm. Moreover, the values of $R_L \to 0$ whatever the composite, which suggests a very favorable adsorption of dye molecules on these composite materials.

To synthesize, from the different types of adsorbents, MK800-ZnO (1:1) sample is the more efficient for the 3 dyes. This can be explained by the structure of these dyes. To this end, some of these molecules have a higher auxochrome group density than others. This is the case with the DG1 dye which has 5 auxochromic groups, the DB53 dye has 8 auxochromic groups and finally the MR19 dye which has 3 auxochromic groups. In conclusion, the higher the auxochrome group density, the more intense the interaction with the surface of the adsorbent.

## 3.7. Limitations of this study

The study of the development of new composite materials, based on kaolinitic clay modified by ZnO, for the elimination of anionic azo textile dyes by adsorption in aqueous solution, may be limited by several methodological, material and analytical factors.

### 3.7.1. In the methodological framework

The Langmuir and Freundlich adsorption isotherm models used to correlate with the characteristic properties of composite materials and anionic azo dye molecules are based on simplifying assumptions that may not accurately reflect the complexities of the real system.

In terms of experimental conditions, we note that the parameters in the adsorption process such as pH, temperature and stirring speed considerably influencing the interaction between the anionic molecules of azo dye and the different composite materials are not always controlled or standardized to perfection. It should be noted that the adsorption experiments were carried out at room temperature; but this can vary slightly from one experiment to another, from one day to another with the potential consequence of an erroneous result and conclusion on the thermodynamic equilibrium which could thus poorly reflect the feasibility and spontaneous nature of the adsorption process.

### 3.7.2. At the material level

The characteristics of adsorbents in terms of surface properties,

morphology, porosity and adsorption capacity can vary slightly. It is sometimes difficult to accurately reproduce the same preparation when moving from one sample to another. It may also happen that the composite material degrades during the experiment; this can the case for example with the release of zinc in solution during experiments, when it is used several times in a row, which can thus affect the adsorption capacities.

#### 3.7.3. On the analytical level

The precision and sensitivity of the spectrophotometer, for measuring optical densities in the UV-VIS range, after the adsorbent is separated from the solution by centrifugation, may be a limitation in the context of this study to determine low concentrations of pollutants (MR19, DB53 and DG1). In this case, measuring the exact quantity of adsorbed dye may prove difficult.

### 3.8. Statistical analysis and significance of the results

It should be emphasized that the scientific assertions, theories, hypotheses and even the methodology used in this study are credible because the results leading to their formulation are reproducible. At this level it is necessary to remember that the methodology leading to the different treatments (thermal, DMSO, acid and thermal + acid) of raw kaolinite with the aim of causing activation of the latter is clearly set out in the literature. The same is true for the immobilization of ZnO on a clay matrix by the sol-gel and co-precipitation processes, with a view to obtaining the different composite materials.

In addition, the adsorption experiments (influence of contact time, influence of initial concentration), which made it possible to carry out the kinetic and isothermal studies of adsorption as part of this work, were carried out in triplicate for each of the samples. It is the same with the measurement of the zeta potential of each of the different samples of raw kaolinite and composite materials.

From the statistical analysis, it appears that the results obtained during the study of the pseudo-second order kinetic model are significant because the linear correlation coefficient values ($R^2$) recorded are all greater than 0.99. In addition, although the values of adsorption capacities at equilibrium ($q_e$), obtained during the experiments are close to those calculated at equilibrium ($q_m$) from this model, it is clear that they remain lower than the latter.

## 4. Conclusion

In this work, natural kaolinitic clay extracted from Cameroon is modified with ZnO, DMSO, and with thermal and acidic treatment to enhance its adsorption properties for water depollution.

ZnO nanoparticles, synthesized by the sol-gel process, are immobilized on the clay material producing a composite ZnO-clay material. After doping with ZnO, a sudden inversion of the nature of the surface charge of certain composite materials (KAODMSO-ZnO, MK600-ZnO, MK700-ZnO, MK800-ZnO) obtained was observed, through zeta potential values ranging from −31 mV before doping with ZnO to +36 mV after doping. The calcination of kaolinite at temperatures above 500 °C and its treatment with DMSO were necessary for the amorphization and separation of the interlayer space. In addition, these operations are also decisive steps in the process of reversing the nature of surface charges.

Compared to natural kaolinite, the nanocomposites showed much higher removal capacities for the anionic textile dyes MR19, DB53 and DG1. In addition, the efficiency of adsorption strongly depends on the zeta potential of the material: the higher the zeta potential is towards positive values, the better the adsorption capacities of the samples towards these anionic textile dyes. The immobilization on an activated kaolinite clay of ZnO, which is located on the border between a covalent polar semiconductor and an ionic semiconductor, is an innovative technique making it possible to considerably improve the adsorption capacity of anionic dyes by kaolinite. Furthermore, the adsorption kinetics of dyes could be well described using the pseudo-second order kinetic model. The adsorption of MR19, DB53 and DG1 on the nanocomposites could be described using the Langmuir model, suggesting that monolayer adsorption took place in all cases.

## Ethical approval

The authors declare that they have no known competing financial interests or personal relationships that could have appeared to influence the work reported in this paper.

## Consent to participate

All authors agreed to participate in this work.

## Consent to publish

All authors agreed to this version for publication.

## CRediT authorship contribution statement

**Pierre Ngue Song:** Writing – review & editing, Writing – original draft, Methodology, Investigation, Formal analysis, Conceptualization. **Julien G. Mahy:** Writing – review & editing, Writing – original draft, Supervision, Methodology, Formal analysis. **Antoine Farcy:** Writing – review & editing, Investigation, Formal analysis. **Cédric Calberg:** Writing – review & editing, Investigation, Formal analysis. **Nathalie Fagel:** Writing – review & editing, Supervision, Project administration, Methodology, Formal analysis. **Stéphanie D. Lambert:** Writing – review & editing, Supervision, Project administration, Methodology, Funding acquisition, Conceptualization.

## Declaration of competing interest

The authors declare that they have no known competing financial interests or personal relationships that could have appeared to influence the work reported in this paper.

## Data availability

Data will be made available on request.

## Acknowledgments

The authors acknowledge Joel Otten and Nicolas Delmelle for their technical support. Julien G. Mahy and Stéphanie D. Lambert thank the F.R.S.-FNRS for their Postdoctoral Researcher position and Research Director position, respectively.

## Appendix A. Supplementary data

Supplementary data to this article can be found online at https://doi.org/10.1016/j.rsurfi.2024.100255.

## References

Ahmad, A., Mustafa, G., Rana, A., Zia, A.R., 2023. Improvements in bioremediation agents and their modified strains in mediating environmental pollution. Curr. Microbiol. 80, 208. https://doi.org/10.1007/s00284-023-03316-x.

Ahmed, S.M., 1966. Studies of the dissociation of oxide surfaces at the liquid-solid interface. Can. J. Chem. 44, 1663–1670. https://doi.org/10.1139/v66-251.

Akkari, M., Aranda, P., Belver, C., Bedia, J., Ben Haj Amara, A., Ruiz-Hitzky, E., 2018. ZnO/sepiolite heterostructured materials for solar photocatalytic degradation of pharmaceuticals in wastewater. Appl. Clay Sci. 156, 104–109. https://doi.org/10.1016/j.clay.2018.01.021.

Aragaw, T.A., Alene, A.N., 2022. A comparative study of acidic, basic, and reactive dyes adsorption from aqueous solution onto kaolin adsorbent: effect of operating parameters, isotherms, kinetics, and thermodynamics. Emerging Contam. 8, 59–74. https://doi.org/10.1016/j.emcon.2022.01.002.

Artifon, W., Cesca, K., de Andrade, C.J., Ulson de Souza, A.A., de Oliveira, D., 2021. Dyestuffs from textile industry wastewaters: trends and gaps in the use of bioflocculants. Process Biochem. 111, 181–190. https://doi.org/10.1016/j.procbio.2021.10.030.

Ashraf, R., Riaz, S., Kayani, Z.N., Naseem, S., 2015. Effect of calcination on properties of ZnO nanoparticles. In: Mater Today Proc. Elsevier Ltd, pp. 5468–5472. https://doi.org/10.1016/j.matpr.2015.11.071.

Belver, C., Bañares Muñoz, M.A., Vicente, M.A., 2002. Chemical activation of a kaolinite under acid and alkaline conditions. Chem. Mater. 14, 2033–2043. https://doi.org/10.1021/cm0111736.

Benkhaya, S., Lgaz, H., Chraibi, S., Alrashdi, A.A., Rafik, M., Lee, H.S., El Harfi, A., 2021. Polysulfone/Polyetherimide Ultrafiltration composite membranes constructed on a three-component Nylon-fiberglass-Nylon support for azo dyes removal: experimental and molecular dynamics simulations. Colloids Surf. A Physicochem. Eng. Asp. 625, 126941 https://doi.org/10.1016/j.colsurfa.2021.126941.

Bera, S.P., Tank, S.K., 2021. Screening and identification of newly isolated Pseudomonas sp. for biodegrading the textile azo dye C.I. Procion Red H-3B. J. Appl. Microbiol. 130, 1949–1959. https://doi.org/10.1111/jam.14920.

Berkani, M., Kadmi, Y., Bouchareb, M.K., Bouhelassa, M., Bouzaza, A., 2020. Combinatıon of a Box-Behnken design technique with response surface methodology for optimization of the photocatalytic mineralization of C.I. Basic Red 46 dye from aqueous solution. Arab. J. Chem. 13, 8338–8346. https://doi.org/10.1016/j.arabjc.2020.05.013.

Bhattacharyya, K.G., SenGupta, S., Sarma, G.K., 2014. Interactions of the dye, Rhodamine B with kaolinite and montmorillonite in water. Appl. Clay Sci. 99, 7–17. https://doi.org/10.1016/j.clay.2014.07.012.

Biddeci, G., Spinelli, G., Colomba, P., Di Blasi, F., 2023. Halloysite nanotubes and sepiolite for health applications. Int. J. Mol. Sci. 24, 4801. https://doi.org/10.3390/ijms24054801.

Brinza, L., Maftei, A.E., Tascu, S., Brinza, F., Neamtu, M., 2022. Advanced removal of Reactive Yellow 84 azo dye using functionalised amorphous calcium carbonates as adsorbent. Sci. Rep. 12, 3112. https://doi.org/10.1038/s41598-022-07134-2.

Brüschweiler, B.J., Merlot, C., 2017. Azo dyes in clothing textiles can be cleaved into a series of mutagenic aromatic amines which are not regulated yet. Regul. Toxicol. Pharmacol. 88, 214–226. https://doi.org/10.1016/j.yrtph.2017.06.012.

Carmen, Z., Daniela, S., 2012. Textile organic dyes-characteristics, polluting effects and separation/elimination procedures from industrial effluents-A critical overview. In: Organic Pollutants Ten Years after the Stockholm Convention—Environmental and Analytical Update. InTech, pp. 55–86. www.intechopen.com.

Chen, G., Li, X., Zhao, H., Qiu, M., Xia, S., Yu, L., 2022. Revealing the mechanisms of mercury adsorption on metal-doped kaolinite(001) surfaces by first principles. J. Hazard Mater. 431, 128586 https://doi.org/10.1016/j.jhazmat.2022.128586.

Chérif, I., Dkhil, Y.O., Smaoui, S., Elhadef, K., Ferhi, M., Ammar, S., 2023. X-ray diffraction analysis by modified Scherrer, Williamson–Hall and size–strain plot methods of ZnO nanocrystals synthesized by oxalate route: a potential antimicrobial candidate against foodborne pathogens. J. Cluster Sci. 34, 623–638. https://doi.org/10.1007/s10876-022-02248-z.

Chung, K.-T., 2016. Azo dyes and human health: a review. Journal of Environmental Science and Health 34, 233–261. https://doi.org/10.1080/10590501.2016.1236602. Part C.

Cuisset, O., 1980. Rapport de recherche LPC N° 96 Propriétés électrocinétiques des particules argileuses Application de la méthode électrophorétique aux prioblèmes d'environnement et d'identification des sols. www.ifsttar.fr.

Deschanvres, J.L., Rey, P., Delabouglise, G., Labeau, M., Joubert, J.C., Peuzin, J.C., 1992. Characterization of piezoelectric properties of zinc oxide thin films deposited on silicon for sensors applications. Sensor. Actuator. 33, 43–45. https://doi.org/10.1016/0924-4247(92)80223-P.

Dihom, H.R., Al-Shaibani, M.M., Radin Mohamed, R.M.S., Al-Gheethi, A.A., Sharma, A., Bin Khamidun, M.H., 2022. Photocatalytic degradation of disperse azo dyes in textile wastewater using green zinc oxide nanoparticles synthesized in plant extract: a critical review. J. Water Process Eng. 47, 102705 https://doi.org/10.1016/j.jwpe.2022.102705.

El Hassani, A.A., Tanji, K., El Mrabet, I., Fahoul, Y., El Gaidoumi, A., Benjelloun, A.T., Sfaira, M., Zaitan, H., Kherbeche, A., 2023. A combined molecular dynamics simulation, DFT calculations, and experimental study of the adsorption of Rhodamine B dye on kaolinite and hydroxyapatite in aqueous solutions. Surface. Interfac. 36, 102647 https://doi.org/10.1016/j.surfin.2023.102647.

Florêncio, T. de M., de Godoi, L.A.G., Rocha, V.C., Oliveira, J.M.S., Motteran, F., Gavazza, S., Vicentine, K.F.D., Damianovic, M.H.R.Z., 2021. Anaerobic structured-bed reactor for azo dye decolorization in the presence of sulfate ions. J. Chem. Technol. Biotechnol. 96, 1700–1708. https://doi.org/10.1002/jctb.6695.

Fumba, G., Essomba, J.S., Merlain Tagne, G., Nsami, J.N., Désiré, P., Bélibi, B., Mbadcam, J.K., 2014. Equilibrium and kinetic adsorption studies of methyl orange from aqueous solutions using kaolinite, metakaolinite and activated geopolymer as low cost adsorbents. Journal of Academia and Industrial Research (JAIR) 3, 156.

Gardolinski, J.E., Carrera, L.C.M., Cantao, M.P., Wypych, F., 2000. Layered polymer-kaolinite nanocomposites. J. Mater. Sci. 35, 3113–3119. https://doi.org/10.1023/A:1004820003253.

Golsheikh, A.M., Kamali, K.Z., Huang, N.M., Zak, A.K., 2018. Effect of calcination temperature on performance of ZnO nanoparticles for dye-sensitized solar cells. Powder Technol. 329, 282–287. https://doi.org/10.1016/j.powtec.2017.11.065.

Gou, Z., Hopla, G.A., Yao, M., Cui, B., Su, Y., Rinklebe, J., Sun, C., Chen, G., Ma, N.L., Sun, Y., 2022. Removal of dye pollution by an oxidase derived from mutagenesis of the Deuteromycete Myrothecium with high potential in industrial applications. Environ. Pollut. 310, 119726 https://doi.org/10.1016/j.envpol.2022.119726.

Goud, B.S., Cha, H.L., Koyyada, G., Kim, J.H., 2020. Augmented biodegradation of textile azo dye effluents by plant endophytes: a sustainable, eco-friendly alternative. Curr. Microbiol. 77, 3240–3255. https://doi.org/10.1007/s00284-020-02202-0.

Hai, Y., Li, X., Wu, H., Zhao, S., Deligeer, W., Asuha, S., 2015. Modification of acid-activated kaolinite with TiO2 and its use for the removal of azo dyes. Appl. Clay Sci. 114, 558–567. https://doi.org/10.1016/j.clay.2015.07.010.

Han, G., Du, Y., Huang, Y., Wang, W., Su, S., Liu, B., 2022. Study on the removal of hazardous Congo red from aqueous solutions by chelation flocculation and precipitation flotation process. Chemosphere 289, 133109. https://doi.org/10.1016/j.chemosphere.2021.133109.

He, H., Tao, Q., Zhu, J., Yuan, P., Shen, W., Yang, S., 2013. Silylation of clay mineral surfaces. Appl. Clay Sci. 71, 15–20. https://doi.org/10.1016/j.clay.2012.09.028.

Henderson, R.K., Parsons, S.A., Jefferson, B., 2008. Successful removal of algae through the control of zeta potential. Separ. Sci. Technol. 1653–1666. https://doi.org/10.1080/01496390801973771.

Hernández-Zamora, M., Martínez-Jerónimo, F., 2019. Exposure to the azo dye Direct blue 15 produces toxic effects on microalgae, cladocerans, and zebrafish embryos. Ecotoxicology 28, 890–902. https://doi.org/10.1007/s10646-019-02087-1.

Ho, Y.S., Mckay, G., 1999. Pseudo-second order model for sorption processes. Process Biochem. 34, 451–465. https://doi.org/10.1016/S0032-9592(98)00112-5.

Ikram, M., Naeem, M., Zahoor, M., Hanafiah, M.M., Oyekanmi, A.A., Ullah, R., Farraj, D. A.A., Elshikh, M.S., Zekker, I., Gulfam, N., 2022. Biological degradation of the azo dye basic orange 2 by Escherichia coli: a sustainable and ecofriendly approach for the treatment of textile wastewater. Water (Switzerland) 14, 2063. https://doi.org/10.3390/w14132063.

Jia, X., Cheng, H., Zhou, Y., Zhang, S., Liu, Q., 2019. Time-efficient preparation and mechanism of methoxy-grafted kaolinite via acid treatment and heating. Appl. Clay Sci. 174, 170–177. https://doi.org/10.1016/j.clay.2019.04.001.

Kahr, G., Madsen, F.T., 1995. Determination of the cation exchange capacity and the surface area of bentonite, illite and kaolinite by methylene blue adsorption. Appl. Clay Sci. 9, 327–336. https://doi.org/10.1016/0169-1317(94)00028-O.

Kamble, S., Agrawal, S., Cherumukkil, S., Sharma, V., Jasra, R.V., Munshi, P., 2022. Revisiting zeta potential, the key feature of interfacial phenomena, with applications and recent advancements. ChemistrySelect 7, e202103084. https://doi.org/10.1002/slct.202103084.

Kenne Diffo, B.B., Elimbi, A., Cyr, M., Dika Manga, J., Tchakoute Kouamo, H., 2015. Effect of the rate of calcination of kaolin on the properties of metakaolin-based geopolymers. Journal of Asian Ceramic Societies 3, 130–138. https://doi.org/10.1016/j.jascer.2014.12.003.

Khader, E.H., Khudhur, R.H., Abbood, N.S., Albayati, T.M., 2023. Decolourisation of anionic azo dye in industrial wastewater using adsorption process: investigating operating parameters. Environmental Processes 10, 34. https://doi.org/10.1007/s40710-023-00646-7.

Khalifa, A.Z., Pontikes, Y., Elsen, J., Cizer, Ö., 2019. Comparing the reactivity of different natural clays under thermal and alkali activation. RILEM Technical Letters 4, 74–80. https://doi.org/10.21809/rilemtechlett.2019.85.

Leal, P.V.B., Pereira, D.H., Papini, R.M., Magriotis, Z.M., 2021. Effect of dimethyl sulfoxide intercalation into kaolinite on etheramine adsorption: experimental and theoretical investigation. J. Environ. Chem. Eng. 9, 105503 https://doi.org/10.1016/j.jece.2021.105503.

Lenarda, M., Storaro, L., Talon, A., Moretti, E., Riello, P., 2007. Solid acid catalysts from clays: preparation of mesoporous catalysts by chemical activation of metakaolin under acid conditions. J. Colloid Interface Sci. 311, 537–543. https://doi.org/10.1016/j.jcis.2007.03.015.

Lu, T., Gilfedder, B.S., Peng, H., Niu, G., Frei, S., 2021. Effects of clay minerals on the transport of nanoplastics through water-saturated porous media. Sci. Total Environ. 796, 148982 https://doi.org/10.1016/j.scitotenv.2021.148982.

Mahy, J.G., Lambert, S.D., Léonard, G.L.M., Zubiaur, A., Olu, P.Y., Mahmoud, A., Boschini, F., Heinrichs, B., 2016. Towards a large scale aqueous sol-gel synthesis of doped TiO2: study of various metallic dopings for the photocatalytic degradation of p-nitrophenol. J. Photochem. Photobiol. Chem. 329, 189–202. https://doi.org/10.1016/j.jphotochem.2016.06.029.

Mahy, J.G., Lejeune, L., Haynes, T., Body, N., De Kreijger, S., Elias, B., Marcilli, R.H.M., Fustin, C.A., Hermans, S., 2021. Crystalline ZnO photocatalysts prepared at ambient temperature: influence of morphology on p-nitrophenol degradation in water. Catalysts 11, 1182. https://doi.org/10.3390/catal11101182.

Mahy, J.G., Mbognou, M.H.T., Léonard, C., Fagel, N., Woumfo, E.D., Lambert, S.D., 2022. Natural clay modified with ZnO/TiO2 to enhance pollutant removal from water. Catalysts 12, 148. https://doi.org/10.3390/catal12020148.

Marin, E., Calderon, A., Diaz, D., 2009. Thermal characterization of ZnO-DMSO (dimethyl sulfoxide) colloidal dispersions using the inverse photopyroelectric technique. Anal. Sci. 25, 705–709. https://doi.org/10.2116/analsci.25.705.

Mbey, J.A., Thomas, F., Ngally Sabouang, C.J., Liboum, Njopwouo, D., 2013. An insight on the weakening of the interlayer bonds in a Cameroonian kaolinite through DMSO intercalation. Appl. Clay Sci. 83–84, 327–335. https://doi.org/10.1016/j.clay.2013.08.010.

Misra, A.J., Das, S., Habeeb Rahman, A.P., Das, B., Jayabalan, R., Behera, S.K., Suar, M., Tamhankar, A.J., Mishra, A., Lundborg, C.S., Tripathy, S.K., 2018. Doped ZnO nanoparticles impregnated on Kaolinite (Clay): a reusable nanocomposite for photocatalytic disinfection of multidrug resistant Enterobacter sp. under visible light. J. Colloid Interface Sci. 530, 610–623. https://doi.org/10.1016/j.jcis.2018.07.020.

Mkaouar, S., Maherzi, W., Pizette, P., Zaitan, H., Benzina, M., 2019. A comparative study of natural Tunisian clay types in the formulation of compacted earth blocks. J. Afr. Earth Sci. 160, 103620 https://doi.org/10.1016/j.jafrearsci.2019.103620.

Mustapha, S., Tijani, J.O., Ndamitso, M.M., Abdulkareem, S.A., Shuaib, D.T., Mohammed, A.K., Sumaila, A., 2020. The role of kaolin and kaolin/ZnO nanoadsorbents in adsorption studies for tannery wastewater treatment. Sci. Rep. 10, 13068 https://doi.org/10.1038/s41598-020-69808-z.

Németh, J., Rodríguez-Gattorno, G., Díaz, D., Vázquez-Olmos, A.R., Dékany, I., 2004. Synthesis of ZnO nanoparticles on a clay mineral surface in dimethyl sulfoxide medium. Langmuir 20, 2855–2860. https://doi.org/10.1021/la035097s.

Ngo, A.C.R., Tischler, D., 2022. Microbial degradation of azo dyes: approaches and prospects for a hazard-free conversion by microorganisms. Int. J. Environ. Res. Publ. Health 19, 4740. https://doi.org/10.3390/ijerph19084740.

Páez, C.A., Contreras, M.S., Léonard, A., Blacher, S., Olivera-Fuentes, C.G., Pirard, J.P., Job, N., 2012. Effect of CO 2 activation of carbon xerogels on the adsorption of methylene blue. Adsorption 18, 199–211. https://doi.org/10.1007/s10450-012-9394-2.

Paquini, L.D., Marconsini, L.T., Profeti, L.P.R., Campos, O.S., Profeti, D., Ribeiro, J., 2023. An overview of electrochemical advanced oxidation processes applied for the removal of azo-dyes. Braz. J. Chem. Eng. 40, 623–653. https://doi.org/10.1007/s43153-023-00300-7.

Paredes-Quevedo, L.C., Castellanos, N.J., Carriazo, J.G., 2021. Influence of porosity and surface area of a modified kaolinite on the adsorption of basic red 46 (BR-46). Water Air Soil Pollut. 232, 509. https://doi.org/10.1007/s11270-021-05450-3.

Paździor, K., Bilińska, L., Ledakowicz, S., 2019. A review of the existing and emerging technologies in the combination of AOPs and biological processes in industrial textile wastewater treatment. Chem. Eng. J. 376, 120597 https://doi.org/10.1016/j.cej.2018.12.057.

Ptáček, P., Kubátová, D., Havlica, J., Brandštetr, J., Šoukal, F., Opravil, T., 2010. The non-isothermal kinetic analysis of the thermal decomposition of kaolinite by thermogravimetric analysis. Powder Technol. 204, 222–227. https://doi.org/10.1016/j.powtec.2010.08.004.

Rasmidi, R., Duinong, M., Chee, F.P., 2021. Radiation damage effects on zinc oxide (ZnO) based semiconductor devices– a review. Radiat. Phys. Chem. 184, 109455 https://doi.org/10.1016/j.radphyschem.2021.109455.

Ravadelli, M., Da Costa, R.E., Lobo-Recio, M.A., Akaboci, T.R.V., Bassin, J.P., Lapolli, F. R., Belli, T.J., 2021. Anoxic/oxic membrane bioreactor assisted by electrocoagulation for the treatment of azo-dye containing wastewater. J. Environ. Chem. Eng. 9, 105286 https://doi.org/10.1016/j.jece.2021.105286.

Ribeiro, M.C.M., Starling, M.C.V.M., Leão, M.M.D., de Amorim, C.C., 2017. Textile wastewater reuse after additional treatment by Fenton's reagent. Environ. Sci. Pollut. Control Ser. 24, 6165–6175. https://doi.org/10.1007/s11356-016-6921-9.

Ruiz-Hitzky, E., Aranda, P., Akkari, M., Khaorapapong, N., Ogawa, M., 2019. Photoactive nanoarchitectures based on clays incorporating TiO2 and ZnO nanoparticles. Beilstein J. Nanotechnol. 10, 1140–1156. https://doi.org/10.3762/BJNANO.10.114.

Selvaraj, V., Swarna Karthika, T., Mansiya, C., Alagar, M., 2021. An over review on recently developed techniques, mechanisms and intermediate involved in the advanced azo dye degradation for industrial applications. J. Mol. Struct. 1224, 129195 https://doi.org/10.1016/j.molstruc.2020.129195.

Silva, M.S.E., Lages, A.S., Santana, G.P., 2017. Physical and chemical study of lattice kaolinites and their interaction with orthophosphate. An. Acad. Bras. Cienc. 89, 1391–1401. https://doi.org/10.1590/0001-3765201720160519.

Song, P.N., Mahy, J.G., Calberg, C., Farcy, A., Caucheteux, J., Fagel, N., Lambert, S.D., 2023. Influence of thermal and acidic treatments on the morphology of a natural kaolinitic clay mineral. Results in Surfaces and Interfaces 12, 100131. https://doi.org/10.1016/j.rsurfi.2023.100131.

Staroń, A., 2023. Sorption and photocatalysis of dyes on an oil-based composite enriched with nanometric ZnO and TiO2. Sustainability 15, 11874. https://doi.org/10.3390/su151511874.

Tang, W., Zhang, S., Sun, J., Li, H., Liu, X., Gu, X., 2017. Effects of surface acid-activated kaolinite on the fire performance of polypropylene composite. Thermochim. Acta 648, 1–12. https://doi.org/10.1016/j.tca.2016.12.007.

Tizazu, S., Tesfaye, G., Wang, A., Guadie, A., Andualem, B., 2023. Microbial diversity, transformation and toxicity of azo dye biodegradation using thermo-alkaliphilic microbial consortia. Heliyon 9, e16857. https://doi.org/10.1016/j.heliyon.2023.e16857.

Turer, D., 2007. Effect of heavy metal and alkali contamination on the swelling properties of kaolinite. Environ. Geol. 52, 421–425. https://doi.org/10.1007/s00254-006-0557-x.

V Panasiuk, Y., Raevskaya, O.E., Stroyuk, O.L., Kuchmiy, S.Y., Dzhagan, V.M., Hietschold, M., Zahn, D.R.T., 2014. Colloidal ZnO nanocrystals in dimethylsulfoxide: a new synthesis, optical, photo- and electroluminescent properties. Nanotechnology 25, 075601. https://doi.org/10.1088/0957-4484/25/7/075601.

Vaiano, V., Sacco, O., Libralato, G., Lofrano, G., Siciliano, A., Carraturo, F., Guida, M., Carotenuto, M., 2020. Degradation of anionic azo dyes in aqueous solution using a continuous flow photocatalytic packed-bed reactor: influence of water matrix and toxicity evaluation. J. Environ. Chem. Eng. 8, 104549 https://doi.org/10.1016/j.jece.2020.104549.

Vane, L.M., Zang, G.M., 1997. Effect of aqueous phase properties on clay particle zeta potential and electro-osmotic permeability: implications for electro-kinetic soil remediation processes. J. Hazard Mater. 55, 22. https://doi.org/10.1016/S0304-3894(97)00010-1.

Yukselen-Aksoy, Y., Kaya, A., 2011. A study of factors affecting on the zeta potential of kaolinite and quartz powder. Environ. Earth Sci. 62, 697–705. https://doi.org/10.1007/s12665-010-0556-9.

Zhang, H., Tian, G., Xiong, D., Yang, T., Wang, S., Sun, Y., Jin, L., Lan, B., Deng, L., Yang, W., Deng, W., 2023. Carrier concentration-dependent interface engineering for high-performance zinc oxide piezoelectric device. J. Colloid Interface Sci. 629, 534–540. https://doi.org/10.1016/j.jcis.2022.08.181.